THESIS

CONTROLS ON GROUNDWATER-SURFACE WATER INTERACTION IN A GLACIAL VALLEY, NORTHERN COLORADO

Submitted by

Valerie Doebley

Department of Geosciences

In partial fulfillment of the requirements

For the Degree of Master of Science

Colorado State University

Fort Collins, Colorado

Summer 2022

Master's Committee:

Advisor: Michael Ronayne

Daniel McGrath
Stephanie Kampf

ABSTRACT

CONTROLS ON GROUNDWATER-SURFACE WATER INTERACTION IN A GLACIAL VALLEY, NORTHERN COLORADO

In the last few decades, scientists determined that groundwater discharge may supply a significant portion of streamflow in mountain watersheds. However, difficulties with access and drilling typically limit the use of monitoring wells to study groundwater in high-elevation, mountainous catchments. The recent installation of two 10-meter-deep monitoring wells plus several riparian wells along the South Fork of the Cache la Poudre River at the Colorado State University Mountain Campus provided an opportunity for a unique hydrogeological study at a mountainous site. Data from these wells combined with numerical groundwater modeling helped quantitively and qualitatively characterize groundwater-surface water exchange along a ~2.7-km study reach.

Analyses reveal complex temporal and spatial variation of gaining and losing stream conditions within the study reach. First, well water level elevations and groundwater modeling results indicate that the South Fork is generally gaining in the upper portion of the valley and losing near the downstream end. We suggest that valley geometry and channel planform influence the spatial differences in groundwater-surface water exchange along the study reach. Second, streamflow differencing and modeling results suggest that the study reach changes between overall gaining and overall losing stream conditions multiple times between May and October. We suggest that these temporal variations in groundwater-surface water exchange are driven by seasonal changes in surface water contributions to streamflow and evapotranspiration.

Third, stable isotope (δ^2H, $\delta^{18}O$) analyses and groundwater modeling results suggest that localized recharge from moraine ponds and stream leakage are important sources of aquifer recharge. These results indicate that groundwater and surface water at the Mountain Campus are highly interdependent, and that any disturbances that impact surface water contributions to streamflow may ultimately impact the groundwater contributions as well.

ACKNOWLEDGEMENTS

I am profoundly grateful to my advisor, Dr. Mike Ronayne, for his mentorship, support, and feedback throughout this entire project. Special thanks to Dr. Dan McGrath and Dr. Stephanie Kampf for serving on my committee and for their insights about this project.

Many thanks to Christoph Suhr, for sharing his knowledge about the geology of the Mountain Campus, which greatly aided in model calibration and developing a conceptual understanding of the study area. I am grateful to Kira Puntenney-Desmond for collecting, compiling, and sharing hydrology data central to this project. I would also like to thank Annie Gegen for her assistance with field work. Thank you to Seth Webb and the Colorado State University Mountain Campus for supporting this work in many ways and for providing frequent updates on the field site during the disruption caused by the Cameron Peak Fire. I would also like to recognize the incredible efforts of the many firefighters who defended the Mountain Campus infrastructure, including the hydrogeology instrumentation, from the impacts of the wildfire.

I would like to express my appreciation to the donors of the scholarships I received throughout graduate school: the American Water Works Association's Hazen and Sawyer Scholarship, the Colorado Groundwater Association's Harlan Erker Memorial Scholarship, the Robert L. Stollar Scholarship, and the Hill Memorial Fellowship. This project was also funded through a Geological Society of America Graduate Student Research Grant. The generous financial support from these organizations helped make this project and my graduate studies possible.

Finally, I would like to thank my friends and family for their encouragement and support throughout my time in graduate school, especially my mother, Korise, and father, John.

TABLE OF CONTENTS

1. INTRODUCTION

1.1 Background and Study Significance

Water from mountain regions is used by nearly 40% of the world's lowland population, a percentage that is projected to grow in the coming decades (Viviroli et al., 2020). At the same time, mountain regions will face changes to the timing and quantity of surface-level contributions to streamflow (e.g., snowmelt, precipitation runoff) due to climate change (Barnett et al., 2005; Messerli et al., 2004). While much emphasis is placed on studying surface-level contributions to streamflow, these water sources do not provide us with the whole picture. Multiple studies found that significant portions of high-elevation streamflow come from the subsurface (e.g., Clow et al., 2003; Frisbee et al., 2011; Harrington et al., 2018). Unlike surface-level contributions, the seasonal variation and sources of groundwater contributions are not as well understood at high-elevation sites. Without this information, it is hard to predict how groundwater contributions to streamflow will respond to climate change in mountain regions. Additional studies are needed to improve our understanding of the sources and seasonality of groundwater contributions to streams.

Just a few decades ago, many scientists viewed high-elevation catchments as "Teflon basins", areas thought to have little hydrogeologic function (e.g., Williams et al., 2015). It was only in the late 1990s – early 2000s that studies refuted this understanding and uncovered the importance of groundwater-surface water exchange in the amount and quality of surface water in high-elevation catchments (Campbell et al., 1995; Clow et al., 2003). Studies of groundwater storage and flow found that the coarse geologic units (e.g., talus, moraine) at high-elevation sites provide a slower path for snowmelt and precipitation to reach streams (Caballero et al., 2002;

Clow et al., 2003; Roy & Hayashi, 2009). Furthermore, hydrograph separations showed that groundwater was a major contributor to streamflow at some high-elevation sites, especially in autumn after snowmelt has finished (Liu et al., 2004; Hood et al., 2006). The most recent studies indicate that groundwater-surface water interactions are impacted by the unique geologic conditions at diverse high-elevation sites. These studies stress the need for more hydrogeological investigations in a variety of mountainous areas to understand how groundwater sustains streamflow (Arnoux et al., 2020; Christensen et al., 2020).

Past characterizations of high-elevation sites used a range of different hydrogeological and geophysical methods. Water chemistry and tracers helped identify sources of stream and spring water (Roy & Hayashi, 2009; Christensen et al., 2020). Ground penetrating radar (GPR), electrical resistivity tomography (ERT), and seismic refraction provided insight to aquifer structure and the locations of subsurface flow paths (McClymont et al., 2011; Harrington et al., 2018). One key hydrogeologic method not found in most previous high-elevation watershed studies is direct observations of groundwater through deep monitoring wells. Due to the difficulty of access and drilling in mountainous areas, wells are often hand augured and limited to near-channel areas where the water table is shallow. However, previous studies in alpine and subalpine regions stress the importance of well measurements for improved characterizations of groundwater processes and aquifer properties (Roy & Hayashi, 2009; Clow et al., 2003; Langston et al., 2013).

When available, instrumented groundwater wells provide accurate water level data at a high temporal frequency (e.g., sub hourly measurements). Level data may offer valuable calibration targets for numerical groundwater models, allowing modelers to estimate hydraulic conductivities, evapotranspiration (ET), and other properties through the calibration process. A suitable model will have similar values and patterns in the observed and simulated hydraulic heads at well locations. Models constrained using well data in this way allow us to quantify hydrogeological processes with higher certainty.

Additionally, wells allow researchers to directly compare groundwater and surface water chemistry. Past studies successfully used stable isotopes of hydrogen and oxygen to identify groundwater sources, but were limited to surface waters, soil lysimeters, and shallow boreholes (Roy & Hayashi, 2009; Christensen et al., 2020; Arnoux et al., 2020). Deep groundwater wells allow us to use chemical methods in other locations of interest where the groundwater is not naturally discharging onto the surface. This enables direct comparisons of groundwater and surface water chemistry. Such comparisons help track groundwater sources and provide an additional soft calibration target for numerical models.

In 2019, two 10-meter-deep groundwater monitoring wells and several (1 to 2-meter-deep) riparian wells were installed along the South Fork of the Cache la Poudre River at the Colorado State University (CSU) Mountain Campus located over 2,700 m above sea level. Groundwater and surface water instrumentation at this high-elevation site provide the opportunity for a unique hydrogeological study with direct measurements of groundwater chemistry and groundwater levels in wells. These data provide an opportunity to develop a well constrained numerical groundwater model. Both modeling and water chemistry analysis will help predict the sources and temporal variation of groundwater contributions to streamflow at this site.

Furthermore, the valley that contains the CSU Mountain Campus is a compelling location for a groundwater-surface water study because it contributes to an important drinking water source. The Cache la Poudre River provides quality drinking water to Fort Collins, Colorado, and surrounding communities (Collins & Sprague, 2005; Coalition for the Poudre River, 2022a). Like many rivers in Colorado, the Cache la Poudre River's South Fork experiences peak flows during late-spring snowmelt but groundwater's role in maintaining its baseflow is not well understood. Understanding the role of groundwater in sustaining this important water supply is more important than ever, due to imminent threats to this watershed from forest fires (e.g., 2020 Cameron Peak Fire) and predicted decreased snowpack due to climate change (Siirila-Woodburn et al., 2021). Numerical groundwater modeling, constrained by well water levels and chemistry, should provide a quantitative understanding of the groundwater-surface water interaction at this site, including seasonal variations and water sources.

1.2 Study Goal and Objectives

This study's goal is to use numerical groundwater modeling constrained by field data to characterize the groundwater-surface water exchange in a study reach along the South Fork. The objectives of this study are to: (1) collect baseline data to characterize the valley hydrogeology; and (2) to quantitively characterize groundwater-surface water exchange along a ~2.7-km reach of the South Fork and evaluate how that exchange is dependent on valley hydrogeologic characteristics as well as seasonal processes. We hypothesized that there is seasonal variability in groundwater-surface water exchange such that the relative role of groundwater increases throughout the summer following snowmelt. However, this study showed that seasonal variation in groundwater-surface water exchange at this site is much more temporally and spatially complex than hypothesized, with different behaviors modeled along different portions of the study reach.

2. SITE DESCRIPTION

This study was conducted in a ~2.6 km^2 study area along a segment of the South Fork at the CSU Mountain Campus in Larimer County, Colorado (Figure 1). The study area is near the base of a ~40 km^2 watershed, which is characterized by glacial landforms and high-relief mountains with peaks over 3,500 m above sea level. Upgradient from the study area, steep headwater channels converge to form the South Fork and its tributary, Fall Creek. The South Fork and Fall Creek enter a lower gradient valley where they merge, just upstream from the study area. The channel through this valley has a meandering planform (Figure 2).

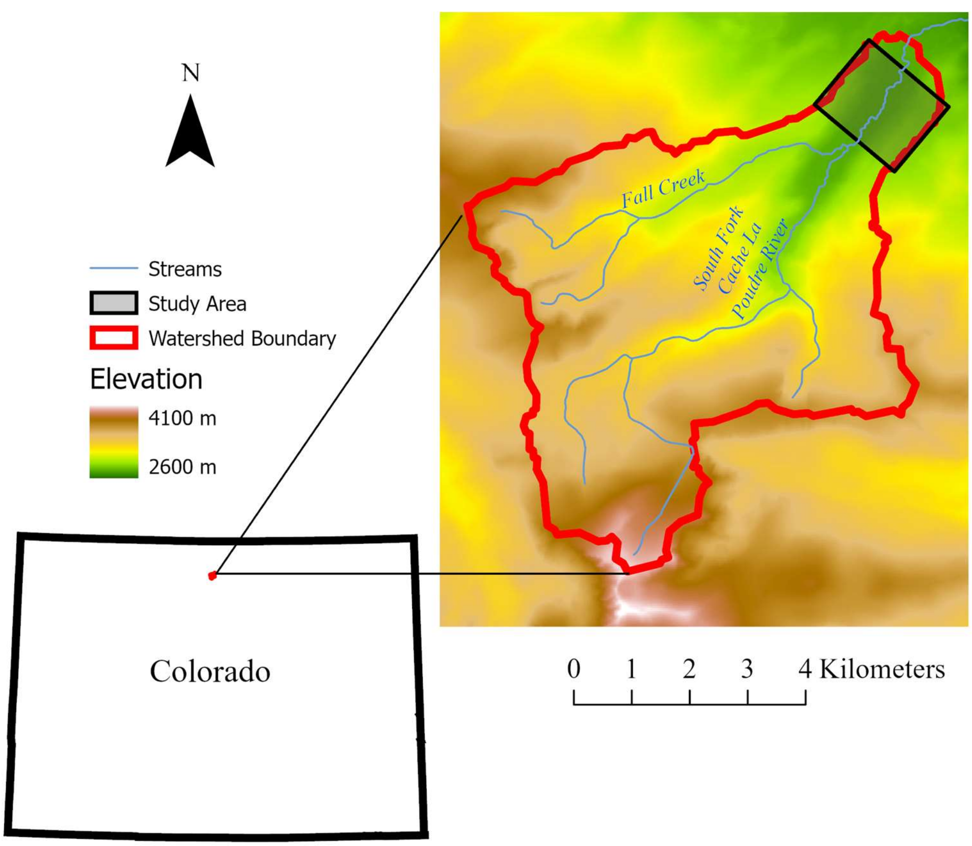

Figure 1: Study area location within the South Fork Poudre Watershed in Colorado. The map projection is NAD 1983 UTM 13N. The DEM raster is from nationalmap.gov. The state outline and stream shapefiles are from Environmental Systems Research Institute (ESRI), accessed via arcgis.com.

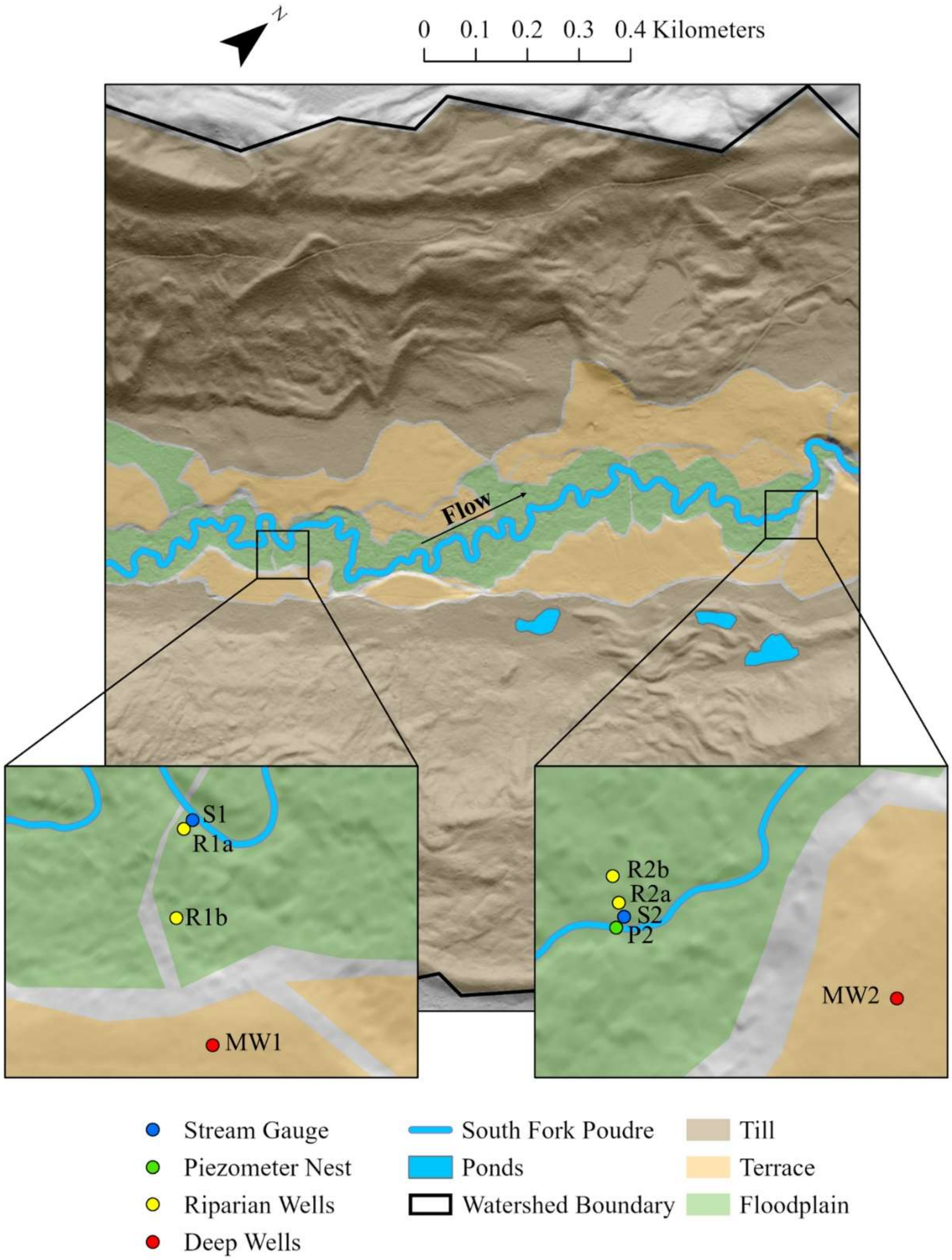

Figure 2: Shaded relief map for the study area with major hydrogeomorphic units (till, terrace, floodplain). Inset maps show locations of monitoring wells and stream gauges at the upstream and downstream transects. The map projection is NAD 1983 UTM 13N. Hydrogeomorphic unit locations for till, terrace, and floodplain come from Suhr (2021). The hill shade was generated with elevation data from the US Geological Survey 3D Elevation Program.

2.1 Hydrogeologic Setting

Glacial and fluvial forces shaped the study area. Glacial expansion and retreat occurred many times in this region, most recently during the Pinedale glaciation, which lasted from ~30 ka – 12 ka (Madole et al., 1998). Glaciation deposited coarse tills and created the many tarns, cirques, and moraines found within this watershed. Near the Mountain Campus, the South Fork flows through a u-shaped, formerly glaciated valley, bounded by two lateral moraines comprised of glacial till. Following glaciation, fluvial forces reworked the sediments in the valley bottom, developing a fluvial terrace and a floodplain (Suhr, 2022).

2.1.1 Hydrogeomorphic Units

Suhr (2021) defined three main hydrogeomorphic units within the study area: till, terrace, and floodplain (Figure 2). The till was deposited during past glaciations and consists of poorly sorted clasts ranging in size from fine sands and silts to boulders (Suhr, 2022). Till forms the lateral moraines bounding the valley segment on two sides. The moraines slope upwards away from the valley bottom, but their hummocky topography has some low-lying areas where surface water collects into small ponds. Some ponds along the southeast moraine appear to have artificially fortified outflows.

Within the valley, terraces border the channel on both sides. Generally flat, the terrace height is about 5 to 8 m above the channel. The surface of the terraces is a thin layer rich in organic matter (Suhr, 2022). Beneath this, terrace sediments are poorly sorted sands and silty sands, according to well logs. Well logs from the southeast side of the valley indicate that the sediment thickness in the terrace areas exceeds 10 meters.

Between the terrace and the channel, there is a low, hummocky floodplain on each side of the channel. This floodplain is subject to regular flooding during snowmelt in the late spring. The floodplain surface is made of fine grains that are deposited when the channel flows over its banks. Under about 0.5 to 1.5 m of this fine sediment, the floodplain is comprised of coarser sands, gravels, and cobbles (Suhr, 2022).

Bedrock is exposed at higher elevations in the watershed, upgradient from the main study area. Although we did not detect the bedrock with the methods used in this study, the study area is known to be underlined by both metamorphic and igneous bedrock. The exposed bedrock in the watershed has been mapped as mica schist [~1710 Ma], gneiss [~1710 Ma], granite [~1400 Ma], granodiorite [~1660 Ma], and pegmatite intrusions from throughout the Early and Middle Proterozoic (Nesse & Braddock, 1989).

2.1.2 Channel and Flow Regime

The South Fork flows from southwest to northeast through the study area. Channel elevation decreases from 2,750 m to 2,743 m along the 1,460-meter length of the study area. The channel through the study area has a highly sinuous, meandering planform; the total channel length through the study area is 2,688 meters, resulting in a sinuosity value of ~1.8. Stream width varies throughout the year and with location but is generally in the range of around 6 to 8 m wide. Channel bed sediments range from sands and gravels to cobbles. Fine-grained point bars are found along the insides of meander bends.

Like most Rocky Mountain streams, the South Fork's hydrograph is dominated by snowmelt, with about 75% of the discharge each year occurring during May through August (Meiman & Leavesley, 1974). Peak flows are typically recorded in June during peak snowmelt in the watershed. Flow decreases throughout the summer, returning to base levels in the late summer and early fall. During the 2020 field season at the Mountain Campus (May through early November), the maximum stream discharge estimated from rating curves was ~427,000 m^3/d (4.9 m^3/s), and the minimum estimated discharge was ~7,000 m^3/d (0.1 m^3/s). During the 2021 field season (May to October), the maximum and minimum discharges were ~586,000 m^3/d (6.8 m^3/s) and ~14,000 m^3/d (0.2 m^3/s), respectively.

2.2 Climate

Meteorological monitoring of the Mountain Campus site occurred sporadically throughout the past several decades. The most extensive reporting of meteorological data for this site occurred during the 1960s and early 1970s. This watershed receives ~540 mm of precipitation per year (1963 – 1971). About 62% of this precipitation comes in the form of snow between October and May (Meiman & Leavesley, 1974). Higher elevations are noted as having greater precipitation intensities and deeper snowpacks. During the summer months, this area experiences convective storms.

Mean annual air temperature is ~ 2°C (Meiman & Leavesley, 1974). Air temperature in this area varies dramatically with time of day and season. July is the warmest month, with mean daily highs of about 21°C and mean daily lows of about 2°C, based on temperature data from 1966 – 1970. February is the coldest month, with mean daily highs of about -1°C and mean daily lows of about -15°C (Meiman & Leavesley, 1974).

Very recently, meteorological monitoring was reinstated at the Mountain Campus. These recent data are accessible online (CSU, 2022a).

2.3 Past and Current Land Use

Native Americans from the Arapaho, Mountain Ute, and Cheyenne tribes were the original inhabitants of the region that includes the study area (CSU, 2022b). After settlers of European descent arrived in the mid-1800s, documented land uses in this area included fur trapping, homesteading, gold prospecting, railroad industry tie making, and logging. Colorado State University received the land that is now the Mountain Campus through a federal land-grant in 1914. Since then, the Mountain Campus hosted a variety of university operations including student learning, academic field camps, conferences, and research.

Today, infrastructure within the study area includes a few dirt roads, academic buildings, a variety of research instrumentation, and cabins owned by CSU and private landowners. The study area is primarily used for academic and research purposes as well as recreation including hiking and fishing.

2.4 Vegetation

Vegetation at this site includes willows, forbs, grasses, and conifer forest. Vegetation type boundaries roughly follow the boundaries of mapped hydrogeomorphic units (Figure 2). The hummocky floodplain was heavily vegetated with grasses and willows (*Salix sp.*), which are subject to frequent flooding during snowmelt. Above the floodplain, the terrace is covered with a mixture of grasses and forbs. The vegetation abruptly transitions to conifer forest on the lateral moraines. Many of the conifer trees on the northwest lateral moraine burned during the Cameron Peak Fire in October of 2020. The conifers on the southeast lateral moraine were not impacted by the wildfire.

3. METHODS

3.1 Instrumentation and Field Data Collection

This study benefitted from previously installed instrumentation located on two transects that intersect the South Fork (Figure 2). The upstream transect includes a stream gauge (S1), a riparian well next to the stream (R1a), another riparian well further from the stream (R1b), and a 10-meter-deep monitoring well on the terrace (MW1). Wells R1a, R1b, and MW1 are all located on the southeast side of the channel at the upstream transect. The downstream transect includes a stream gauge (S2), a set of nested in-stream piezometers (P2), a riparian well next to the stream (R2a), another riparian well further from the stream (R2b), and a 10-meter-deep monitoring well on the terrace (MW2). At the downstream transect, the deep monitoring well is located on the southeast side of the channel and the riparian wells are located on the northwest side of the channel (Figure 2). Table 1 presents the locations and completion information for the wells.

Table 1. Location data and well completion information for monitoring wells used in this study.

Well Name	Well Type	Depth [m]	Screened Length [m]	GPS Coordinates	Elevation* [m amsl]
R1a	Riparian well	2.0	**	40.56061707 -105.597495	2748.4
R1b	Riparian well	1.0	**	40.56044602 -105.5972665	2748.6
MW1	Deep well	10	7.62	40.56030164 -105.5968334	2752.8
R2a	Riparian well	1.3	**	40.56761987 -105.5908277	2744.2
R2b	Riparian well	1.4	**	40.56765321 -105.5909155	2744.2
MW2	Deep well	10	4.57	40.56803716 -105.5899304	2751.1

Notes:
*Elevations are measured at the top of the well casing, in meters above mean sea level (m amsl).
**Riparian wells are slotted over most of their length to serve as water table observation wells.

3.1.1 Water Level Measurements

All wells and both stream gauges were instrumented with pressure transducers to measure water levels. Water levels were measured at deep monitoring wells at a 10-minute interval from May to early fall and at a 30-minute interval during the rest of the year. Water levels in deep monitoring wells were monitored year-round, except for one period in the early spring of 2020 when the pressure transducers ran out of storage. Riparian well and stream water levels were monitored at a 15-minute interval from May to October. Water levels were usually not logged in these locations during winter, due to the stream freezing and the water table dropping below the bottom of most riparian wells in wintertime. The exception is R1a, where a larger water column allowed for year-round monitoring. Water levels of riparian wells at the downstream transect were monitored in May to October of 2021 only.

We validated transducer water level values by comparing them to monthly manual water level measurements. From the water level data, we calculated hydraulic head in meters above sea level, using corrected RTK elevations from GPS survey points at each well and stream gauges. For unconfined aquifers like this one, the water level elevation in wells is equivalent to the water table at that location. Level data from the unvented transducers were corrected for atmospheric pressure fluctuations. Atmospheric pressure was monitored with a Solinst™ barologger deployed near MW1, using a measurement time interval that was consistent with the wells. Atmospheric pressure was converted to a length then subtracted from the total level recorded by transducers.

The nested piezometers were only measured manually because they did not have transducers. Depth to water measurements were compared for the shallow and deep nested piezometers to determine if the stream conditions were gaining or losing. We routinely used a level to check that the tops of the nested piezometers were even, to ensure that depth to water measurements in each piezometer were taken from the same elevation.

3.1.2 Stream Discharge

Discharge data were available for both stream gauges in 2020 and 2021. Between May and October, discharge was periodically manually measured via current metering at the upstream and downstream transects, and rating curves were developed to estimate stream discharge from stage measurements recorded at a 15-minute frequency (K. Puntenney-Desmond, personal communication, Jan 2022).

Streamflow differencing was performed by subtracting the calculated discharge at the upstream station (Q_{S1}) from the calculated discharge at the downstream station (Q_{S2}). A positive difference ($Q_{S2} – Q_{S1} > 0$) indicates a net gain in streamflow between the upstream and downstream stations. A negative difference ($Q_{S2} – Q_{S1} < 0$) indicates a net loss in streamflow.

3.1.3 Hydraulic Conductivities

We estimated aquifer hydraulic conductivities by conducting specific capacity tests at MW1 and MW2. Monitoring wells were pumped continuously using a low-flow pump powered by a marine battery until the water level stabilized. To track stabilization, we manually measured well water level with a water level meter at least once every 4 minutes during pumping. Water level stabilized after 38 minutes at MW1 and after 20 minutes at MW2. Throughout the experiment, pumping rates were monitored using a stopwatch and a 5-gallon bucket with measurement markings. Transmissivity was calculated using the empirical relationship of Razack & Huntly (1991):

$$T = 15.3(\frac{Q}{h_0 - h})^{0.67} \quad \text{(Equation 1)}$$

where T is transmissivity [L^2/T], Q is the pumping rate [L^3/T], h_0 is the initial pre-pumping water level [L], and h is the stabilized water level in the well [L] (Fetter, 2001). Within brackets, L and T represent dimensions of length and time, respectively. Then, hydraulic conductivity was calculated from transmissivity as follows:

$$K = T/b \quad \text{(Equation 2)}$$

where K is hydraulic conductivity [L/T] and b is the well screened interval length [L].

We also estimated streambed hydraulic conductivities using a streambed permeameter. A seal was created at the base by hammering the permeameter into the streambed sediment. To initiate the test, water was added into the permeameter to increase the hydraulic head above stream level. We monitored the water level in the permeameter as it gradually returned to stream level. Water levels were recorded at least once every 30 seconds until the water level in the permeameter either returned to stream level or stabilized, usually after about 5 to 10 minutes. Three replicate streambed permeameter tests were conducted at the downstream transect and at a midpoint along the channel between the transects. Only two replicate tests were conducted at the upstream transect, where the hard, coarse streambed made it difficult to achieve a seal between the base of the permeameter and the streambed. Data were analyzed to estimate streambed hydraulic conductivities using the method outlined in Landon et al. (2001):

$$K_{sb} = \frac{L}{t_1 - t_0} ln \frac{H_0}{H_1} \quad \text{(Equation 3)}$$

where K_{sb} is the streambed hydraulic conductivity [L/T], L is the depth of the pipe into the streambed [L], t_1 - t_0 is the time of the test [T], H_0 is the initial water level [L], and H_1 is the water level at the end of the test [L].

3.1.4 Stable Isotopes

In 2020 and 2021, we collected monthly water samples from June through October for stable isotope analysis. Samples came from deep monitoring wells, stream water, one riparian well (R1a), one of the nested piezometers (P2), and ponds along the southeast moraine.

To collect groundwater samples from the deep monitoring wells, we used a pump powered by a marine battery. At the riparian well and nested piezometers, we used a manual inertial pump constructed from a check valve attached to the end of a length of tubing. Following the methods outlined in Clark & Fritz (1997), we purged at least three well volumes prior to collecting a groundwater sample. Purged volumes were measured using 5-gallon buckets. We rinsed a smaller bucket with sample water three times before collecting each sample. Surface water samples were collected from a fast-flowing (non-eddy) portion of the channel.

All samples were filtered in the field using a 0.22-micrometer filter that attaches to the end of a syringe. We rinsed the syringe with sample water three times before filling the syringe with sample water again and filtering it into a glass vial. Vials were filled above the rim to make sure no air bubbles were trapped. Filters were replaced between samples. For quality assurance, duplicate samples were collected of every fourth water sample. Water samples were placed in a cooler immediately after collection, then transferred to a refrigerator upon returning from the field site.

The monthly water samples and duplicates were analyzed for stable isotopes of oxygen ($\delta^{18}O$) and hydrogen ($\delta^{2}H$) at the University of Utah Stable Isotope Ratio Facility for Environmental Research (SIRFER). Values were reported as permilles (‰) relative to a reference, Vienna Standard Mean Ocean Water (VSMOW):

$$\delta^{18}O_{sample} = \left(\frac{(^{18}O/^{16}O)_{sample}}{(^{18}O/^{16}O)_{reference}} - 1\right) \times 1000\ ‰ \qquad \text{(Equation 4)}$$

$$\delta^{2}H_{sample} = \left(\frac{(^{2}H/^{1}H)_{sample}}{(^{2}H/^{1}H)_{reference}} - 1\right) \times 1000\ ‰ \qquad \text{(Equation 5)}$$

^{1}H, ^{2}H, ^{16}O, and ^{18}O are all naturally occurring stable isotopes found in water. The heavier isotopes, ^{2}H and ^{18}O, are relatively rare, and their relative abundance is a function of temperature during precipitation and evaporative effects (Clark & Fritz, 1997).

The isotope data are plotted alongside a local meteoric water line (LMWL) from Loch Vale, located 30 km south of the study area:

$$\delta^{18}O = 7.818 \times \delta^{2}H + 7.879 \qquad \text{(Equation 6)}$$

This LMWL was generated from 522 precipitation samples collected at Loch Vale by the United States Geological Survey (USGS), downloaded from the National Water Quality Information System (USGS, 2017).

For waters sampled in Colorado, $\delta^{2}H$ and $\delta^{18}O$ values are typically negative. $\delta^{2}H$ and $\delta^{18}O$ values become more negative when they are more depleted of the heavy isotopes, relative to VSMOW. Depletion becomes more pronounced as the temperature during precipitation decreases. Warm-weather precipitation is relatively less depleted (less negative δ values).

Furthermore, evaporation preferentially removes the lighter isotopes, ^{1}H and ^{16}O, leading to relatively higher (less negative) $\delta^{2}H$ and $\delta^{18}O$ values in residual surface waters. This evaporative effect is greater for ^{16}O than it is for ^{1}H. Consequently, residual waters will fall below the LMWL, while waters unaffected by evaporation fall on the LMWL (Clark & Fritz, 1997).

3.2 Groundwater Flow Modeling

A physically based, 3-dimensional numerical groundwater model was developed for the Mountain Campus Site using MODFLOW-2005, a finite-difference code. MODFLOW solves the following partial differential equation for aquifer systems with complex boundaries and parameter distributions (Harbaugh, 2005):

$$\frac{\partial}{\partial x}\left(K_{xx}\frac{\partial h}{\partial x}\right)+\frac{\partial}{\partial y}\left(K_{yy}\frac{\partial h}{\partial y}\right)+\frac{\partial}{\partial z}\left(K_{zz}\frac{\partial h}{\partial z}\right)+W=S_s\frac{dh}{dt} \qquad \text{(Equation 7)}$$

where K_{xx}, K_{yy}, and K_{zz} are hydraulic conductivities in the x, y, and z directions [L/T], which vary with position throughout the model domain; h is hydraulic head [L]; W represents sources or sinks of water (e.g., recharge) as a volumetric flux per unit volume [T^{-1}]; S_s is specific storage [L^{-1}]; and t is time [T].

During steady-state simulations, head does not change with time, so the right side of the governing equation is equal to zero. Furthermore, if we assume that the aquifer material is isotropic within individual grid cells, we can simplify Equation 7 for steady-state flow conditions:

$$\frac{\partial}{\partial x}\left(K\frac{\partial h}{\partial x}\right)+\frac{\partial}{\partial y}\left(K\frac{\partial h}{\partial y}\right)+\frac{\partial}{\partial z}\left(K\frac{\partial h}{\partial z}\right)+W=0 \qquad \text{(Equation 8)}$$

For this study, MODFLOW model scenarios were developed and post-processed using Groundwater Vistas© Software version 8 from Environmental Simulations Inc (Rumbaugh & Rumbaugh, 2020). Groundwater-surface water interaction was modeled using the Streamflow-Routing (SFR) package (Prudic et al., 2004).

3.2.1 Domain and Grid

Establishing a 3D gridded model domain is the first step in developing the groundwater model for the field site. Our model domain is rotated at a 50° azimuth so that gridded rows run parallel to the valley's orientation (Figure 1). The model domain measures 1460 m in the direction of the valley (southwest – northeast), and 1800 m across the valley (southeast – northwest). This domain is divided into 73 columns and 144 rows. Column spacings are 20 meters. Row spacings are 20 m near the top and bottom of the grid, but gradually decrease to 5 m in the area around the channel, allowing for greater resolution to accurately map the highly sinuous path of the meandering channel.

Locations of the upgradient (southwest) and downgradient (northeast) model edges were selected based on several criteria. First, these model boundaries were positioned so that both transects with available data were within the model domain and not directly adjacent to GHB cells. Second, locations of the model edges were positioned so that the channel is roughly perpendicular to the edge, to prevent the highly sinuous channel from leaving and reentering the model domain. Third, the downstream model edge needed to be upgradient from the valley's end, where there are sudden changes in the topography and geology. There are not sufficient field data to constrain the model in this area downstream from the Mountain Campus. For these three reasons, we positioned the model edges as shown in Figures 3 and 4.

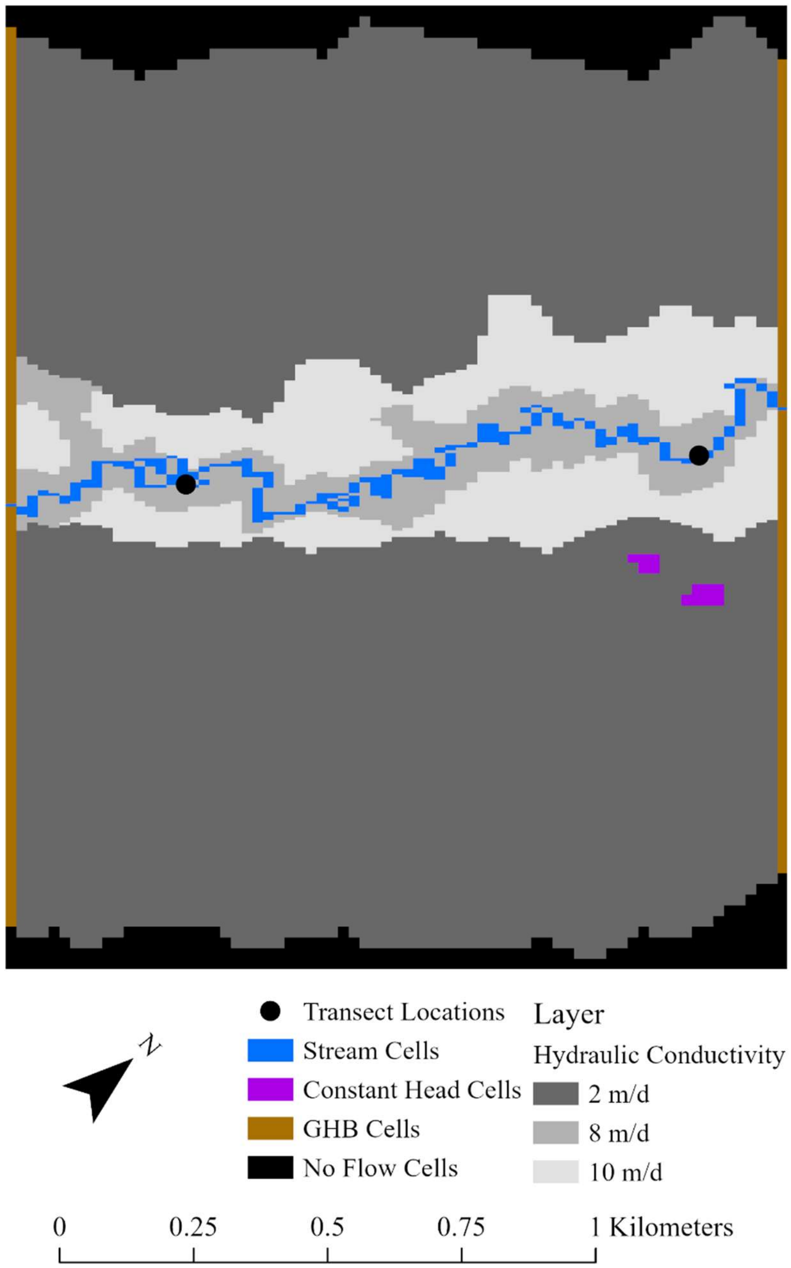

Figure 3: Map of the upper layer of the model domain including stream cells, ponds (constant head), general head boundaries (GHBs), no-flow boundaries, and hydraulic conductivity zones. The locations of the upstream and downstream transects are marked with black dots.

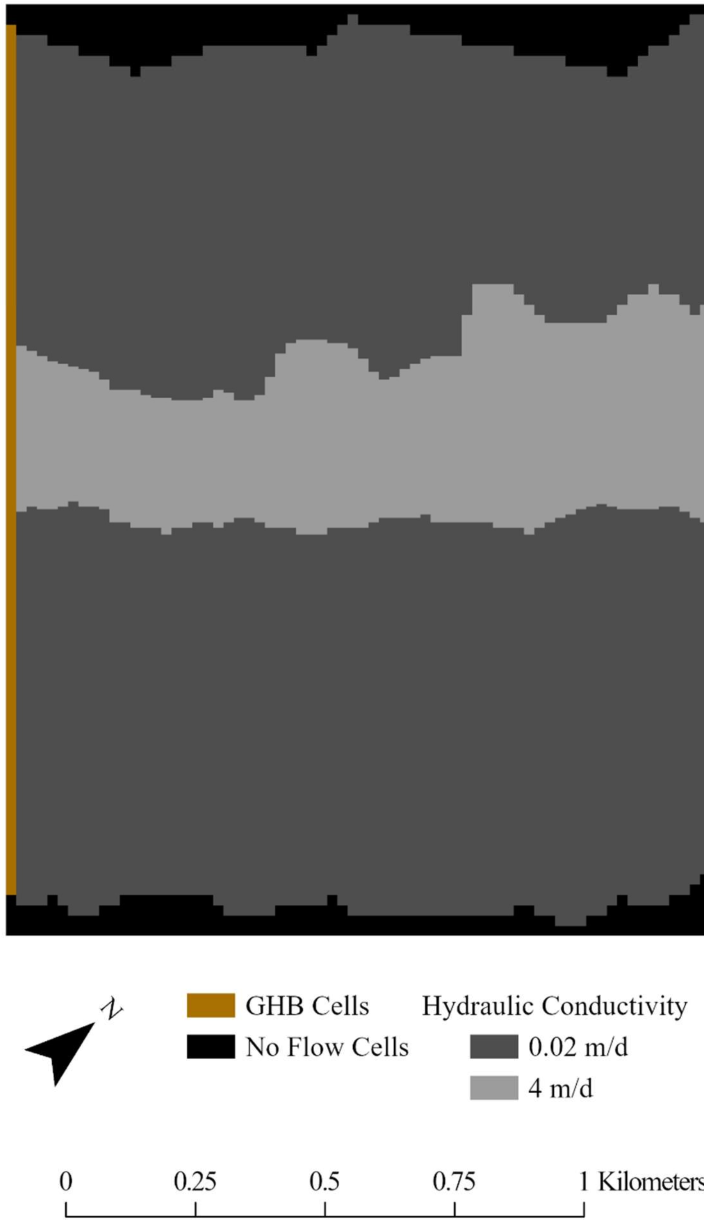

Figure 4: Map of the lower layer of the model domain including general head boundaries (GHBs), no-flow boundaries, and hydraulic conductivity zones.

The total model thickness ranges from approximately 12 m beneath the stream to greater than 200 m along the watershed divides. To allow for the simulation of vertical gradients, the model was discretized using two layers. The boundary between the upper and lower layers was set at the halfway point between the model top elevation and the model bottom elevation in each cell, such that the top of the lower layer is a subdued version of surface topography. In lateral moraines like the ones at this site, layering roughly follows surface topography (Lukas & Sass, 2011).

3.2.2 Boundary Conditions

The top surface of the model comes from lidar-derived land surface elevations. The lidar dataset covering the study area was collected during 2013 and 2014 as part of the USGS 3D Elevation Program (USGS, 2015). The raw lidar dataset has a point density of 4.63 points/m^2 and was gridded to a 1-meter Digital Elevation Model (DEM). The DEM was processed and projected in ArcGIS using the North American Datum 1983 Universal Transverse Mercator 13 North (NAD 83 UTM 13 N) coordinate system. Land surface elevations were extracted at the center node of each model domain grid cell and imported into Groundwater Vistas.

Base elevations for the model domain were more challenging. Although the bedrock depth was observed during drilling of the Mountain Campus water supply well (~ 23 m below ground surface), there are no details on the spatial variability of bedrock depth. Bedrock was not reached while installing the 10-meter-deep wells on the terrace, nor detected by seismic refraction surveys along the terrace (D. McGrath, personal communication, Jan 2021). Seismic profiles along the terrace penetrated to depths of nearly ~12 m but did not detect bedrock. The model bottom elevation for each column was set at 12 m below the streambed elevation in that column. This lower boundary condition is interpreted as a flow line boundary, rather than a well-defined geologic contact.

No-flow boundaries were specified along the watershed divide on the northwestern and southeastern edges of the model (Figure 3). The other two sides of the rectangular model domain are set as head-dependent inflow/outflow boundaries because groundwater may flow through the subsurface into and out of the valley in these locations. These boundary conditions were specified using MODFLOW's general head boundary (GHB) package. The external heads, which control the hydraulic gradient near the model boundary, were estimated using DEM stream elevations 400 m upstream and downstream from the model domain.

The Streamflow-Routing package (Prudic et al., 2004) was used to simulate groundwater-surface water interaction and surface water flow of the South Fork. The channel location was created as a line shapefile in ArcGIS and imported into Groundwater Vistas. 329 model cells along the shapefile's path were classified as stream cells and ordered by reach number from furthest upstream (1) to furthest downstream (329). The streambed elevation at the channel endpoints was determined from the DEM.

In addition to stream cell designations and the assignment of reach numbers, the SFR package requires several other input parameters, including the Manning's roughness, streambed hydraulic conductivity, the incoming streamflow at reach 1 (upgradient edge), and the stream depth in the first and last reaches. Stream depth was set to 0.25 m above the streambed elevation, based on manual stage measurements from the study area. We used a Manning's roughness of 0.035, based on previously published values for a winding channel with some pools, shoals, weeds, and stones (Chow, 1959). Model-specified streambed hydraulic conductivities were set to the average streambed hydraulic conductivity from streambed permeameter tests at the study area (Section 3.1.3). A stream width of 7 m was assigned based on manual stream width measurements at the upstream and downstream transects. The first SFR cell was assigned a streamflow based on discharges measured at the upstream transect stream gauge (S1). For the steady-state model, we used the monthly average discharge at the upstream transect for August

2020. Stream levels and aquifer heads change less dramatically during August; therefore, field data collected during this month were used to develop the steady-state model. A summary of all SFR parameter values is provided in Table 3 in Section 4.3.1, along with other model parameters.

The model also includes cells designated as constant head boundaries. The small ponds along the southeast moraine were assigned as constant head cells. The elevation of each pond was determined using the elevation from the DEM at the edge of the pond. Small fluctuations in pond level are assumed to be negligible.

3.3 Steady-State and Transient Model Simulations

3.3.1 Steady-State Model

A steady-state model was developed to perform initial model calibration. Model parameter values were calibrated using the heads in monitoring wells as calibration targets. To do this, the average hydraulic head value during August 2020 was calculated for each well. The exceptions are the downstream riparian wells (R2a and R2b) which were not monitored in 2020. For these two wells, we used their average heads during August 2021 instead. Model parameters were adjusted to minimize the residuals for each well (i.e., observed value minus simulated value).

Hydraulic conductivity zones (Figures 3 and 4) were based on a geologic map with the locations of till, terrace, and floodplain units in the study area (Suhr, 2021). Initial estimates of hydraulic conductivities came from specific capacity tests at the deep monitoring wells (Section 3.1.3). Hydraulic conductivities for each zone were refined during model calibration.

Diffuse recharge from precipitation was modeled over the entire domain. Two zones were used to implement recharge – one zone encompassing the valley (mapped floodplain and terrace, Figure 2) and another zone on the hillslopes (till extent on moraines, Figure 2). Higher recharge was simulated on the hillslopes. For an upper bound, recharge rates were constrained by precipitation measured at the National Oceanic and Atmospheric Administration (NOAA) weather station at Bear Lake in Rocky Mountain National Park, 28 km south of the study area. A daily precipitation dataset from 2020 was downloaded from the National Centers for Environmental Information website using the Climate Data Online Tool (NOAA, 2020). This dataset was used to calculate an average daily precipitation rate between May and October of 0.0013 m/d. This precipitation rate served as an upper bound on reasonable recharge rates, while calibrating recharge values in both zones.

Modeled ET zones are in the floodplain only, due to the presence of deep-rooted phreatophytes (willows). Direct ET from the saturated zone is assumed to be negligible on the moraines and terraces. Initial estimates of willow ET rates come from the range of values presented by Frédette et al. (2019). Frédette et al. (2019) reports willow ET rates ranging from 0.0007 to 0.0227 m/d. The growing season maximum ET value was refined within this range during calibration of the steady-state model.

3.3.2 Transient Model

Transient simulations help determine seasonal changes in groundwater storage and contributions to streamflow. To investigate these changes, we devised a 5-year transient simulation divided into monthly stress periods, with a goal of replicating the field conditions of May through October 2020. Stress periods are discretized lengths of time; values of selected source/sink fluxes (e.g., incoming streamflow and ET) are changed at the beginning of each stress period. The transient model provides solutions to Equation 7 with site-specific boundary conditions and model parameters.

For the transient model, we used the calibrated parameter values from the steady-state model. These parameter values were held constant across all stress periods, with two exceptions: stream discharge into the first SFR cell and ET.

The stream discharge into the first SFR cell varies between stress periods. Values were assigned based on the monthly average discharge at the S1 stream gauge during May to October 2020 (Table 4). The discharge values measured in October were used for the months of November through April, when stream gauging was not possible due to ice.

ET also varies between stress periods. To simulate winter plant dormancy, we used an ET rate of 0 m/d for November through April. We used our calibrated steady-state model ET value as a maximum ET value in July and August. We gradually tapered ET up to the maximum value during May and June and back down during September and October. All other model parameters are held constant across all stress periods at the values determined during steady-state model calibration.

Transient models also require a few additional inputs beyond those needed for a steady-state model. First, transient models require storage parameters, which are not necessary for steady-state models that do not simulate changes in storage. Aquifer storage parameter (S_y, S_s) values listed in Table 3 in Section 4.3.1 are based on literature values for unconsolidated silty sand aquifer material (Fetter, 2001; Dassargues, 2019). Additionally, transient models require initial conditions. Initial hydraulic heads for the transient simulation come from the solution to the steady-state scenario. A five-year simulation provided enough time for the transient model to converge (i.e., during the simulated time-period, the annual fluctuations in the modeled hydraulic heads started repeating themselves from year to year).

The performance of the transient model was evaluated by comparing simulated and observed hydraulic heads in wells. For each well, we calculated the average hydraulic head for each month from May to October 2020. The exceptions are the downstream riparian wells (R2a and R2b) where 2021 data were used instead because these wells were not monitored in 2020. The observed and simulated hydraulic heads were used to calculate residuals for each well and overall calibration statistics for the transient model.

3.4 Particle Tracking Simulation

As a post-processing step for the steady-state model, we used particle tracking to identify the sources of groundwater arriving at MW2. This analysis was motivated by the unique isotopic composition ($^{2}H/^{1}H$ and $^{18}O/^{16}O$ ratios) of groundwater sampled at MW2, the deep monitoring well near the downstream transect. To perform particle tracking, we used MODPATH (Pollock, 2012), which simulates the movement of particles via advection. Particles are backtracked from MW2 to determine the potential source(s) of the well water. An effective aquifer porosity of 0.15 was used during particle tracking, based on literature values for glacial till (Fetter, 2001).

4. RESULTS

4.1 Field Data Analysis

In general, the field results indicate there are complex gaining and losing stream conditions that vary both temporally and spatially along the South Fork within the study area.

4.1.1 Hydraulic Heads

At the upstream transect, hydraulic heads are highest at MW1 and lowest at the stream during all monitored months (Figure 5). This indicates that the South Fork at the upstream transect is generally gaining (i.e., groundwater flow is directed towards the channel). However, the measured hydraulic heads at the stream and well R1a are roughly equal during June, highlighting the potential for stream recharge to the riparian zone during peak flow. At the downstream transect, the stream and near-stream riparian wells all have roughly equal hydraulic heads from May to October 2021, indicating parallel flow (Figure 5). However, MW2 always has lower hydraulic head than the stream and riparian wells.

A streambed piezometer nest is installed at the downstream transect, although continuous measurements are not available. Manual measurements were only collected in the late summer and fall due to difficulty taking measurements during high flows in May, June, and July. When measurements were possible, the nested piezometers usually indicated losing stream conditions at the downstream transect. In 2020, we observed gaining stream conditions at the nested piezometers in August and losing stream conditions in November. In 2021, we observed losing stream conditions at the nested piezometers in August, September, and October.

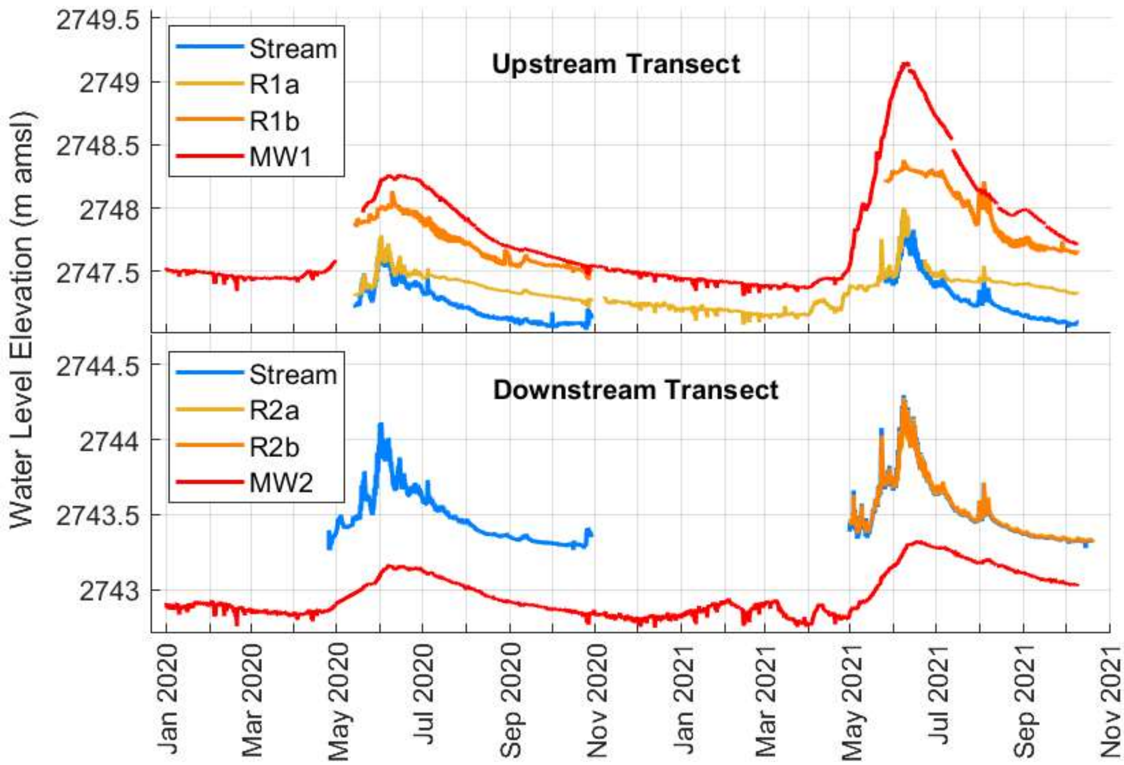

Figure 5: Stream and well water level elevations during 2020 and 2021. At the downstream site in 2021, the stream, R2a, and R2b all plot on top of each other.

4.1.2 Streamflow Differencing

Within the study area, the South Fork alternates between overall gaining and overall losing stream conditions at different times during the period from May to October (Figure 6). In May, there is a net decrease in streamflow between the two gauges (losing stream conditions). During peak runoff in early June, there is a rapid shift to strongly gaining stream conditions. Possible effects from rating curve uncertainty on streamflow differencing during peak flow are discussed in Section 5.2.2. Stream conditions rapidly return to losing by late June, then slowly shift back to gaining stream conditions in August. The stream was gaining through the end of the field season in October. This pattern is very similar in 2020 and 2021.

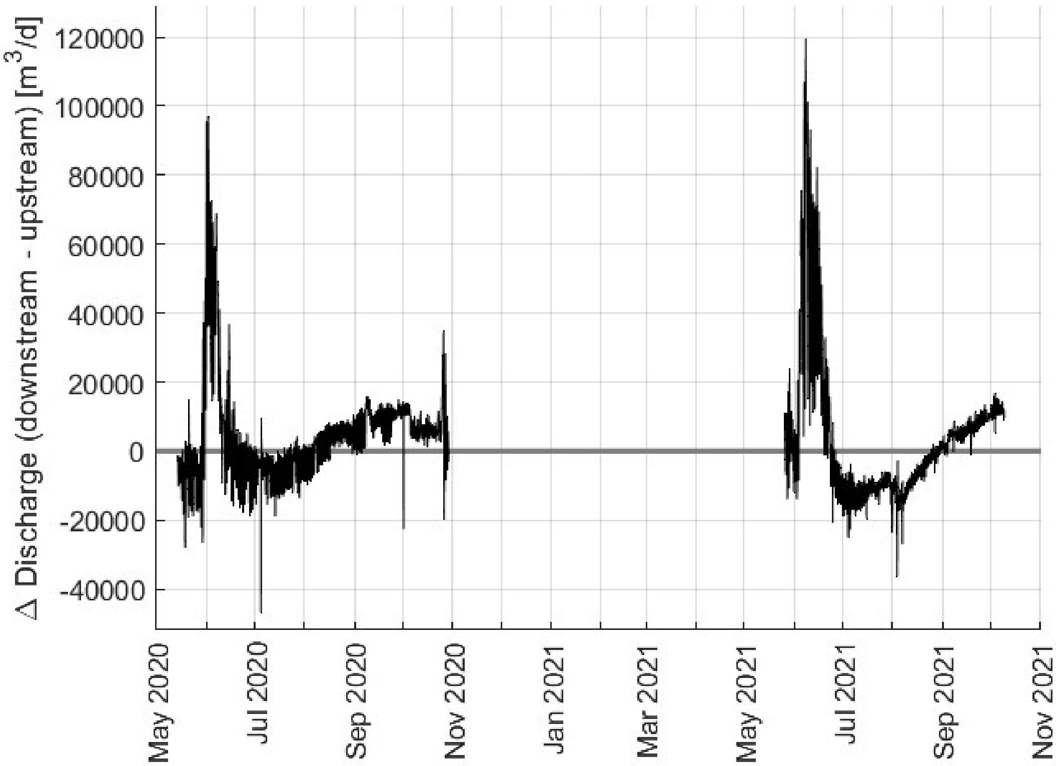

Figure 6: Difference in surface water discharge between the upstream and downstream gauges in 2020 and 2021, calculated as downstream discharge minus upstream discharge. Negative numbers indicate overall losing stream conditions between the gauges. Positive numbers indicate overall gaining stream conditions between the gauges.

In 2020, the peak discharge occurred on May 31 at the upstream transect and June 1 at the downstream transect. The peak streamflow difference was also recorded on June 1 in 2020. In 2021, the peak discharge occurred on June 7 and June 8 at the upstream and downstream transects, respectively. The peak streamflow difference also took place on June 8 in 2021.

4.1.3 Hydraulic Conductivities

Using specific capacity tests, we estimated an aquifer hydraulic conductivity of 4.7 m/d at MW1 and 17.1 m/d at MW2. Streambed hydraulic conductivity measurements ranged from 7.5 to 26.8 m/d, averaging 15.1 m/d (standard deviation = 6.2 m/d).

4.2 Stable Isotopes

During 2020 and 2021, we collected a total of 71 isotope samples from six different source water designations: stream, streambed piezometer, riparian wells, MW1, MW2, and ponds (Table 2). The different source waters generally had different isotopic compositions, although the degree of clustering depended on the month. Furthermore, isotopic compositions vary from month to month for certain source waters. Isotope sample results for select months are shown in Figure 7. Individual plots of isotope samples separated by sampling event are in Appendix A Figures A1 – A9. The following subsections summarize each source water's seasonal patterns, and position relative to other source waters and the LMWL.

Table 2: Summary of stable isotope results. For all locations except the ponds, averages and ranges are based on samples collected monthly during the summer and fall of 2020 and 2021. No samples were collected during September and October 2020 due to the Cameron Peak Fire. Ponds were sampled during October 2021 only.

		δ^2H (‰)		***$\delta^{18}O$ (‰)***	
Source water	***Number***	***Average***	***Range***	***Average***	***Range***
MW1	13	-119	-126 to -111	-15	-17 to -14
MW2	14	-96	-112 to -92	-13	-15 to -12
R1a	12	-124	-127 to -119	-16	-17 to -15
Piezometer	8	-123	-129 to -117	-17	-17 to -15
Stream	22	-125	-136 to -117	-17	-19 to -15
Pond	2	-104	-114 to -94	-13	-15 to -11

4.2.1 Stream Water

Of all the source waters, stream water samples varied the most over the period from June to early fall. Early season stream water samples were the most depleted waters. However, in both 2020 and 2021, stream water became less depleted throughout the summer, reaching its peak isotopic heaviness in August and September. Stream water became slightly more depleted again in October and November (Figure 7). Stream water typically plotted close to or slightly below the LMWL. June stream water plots closer to the LMWL than other months, indicating that the smallest influence of evaporation on stream water occurs at this time.

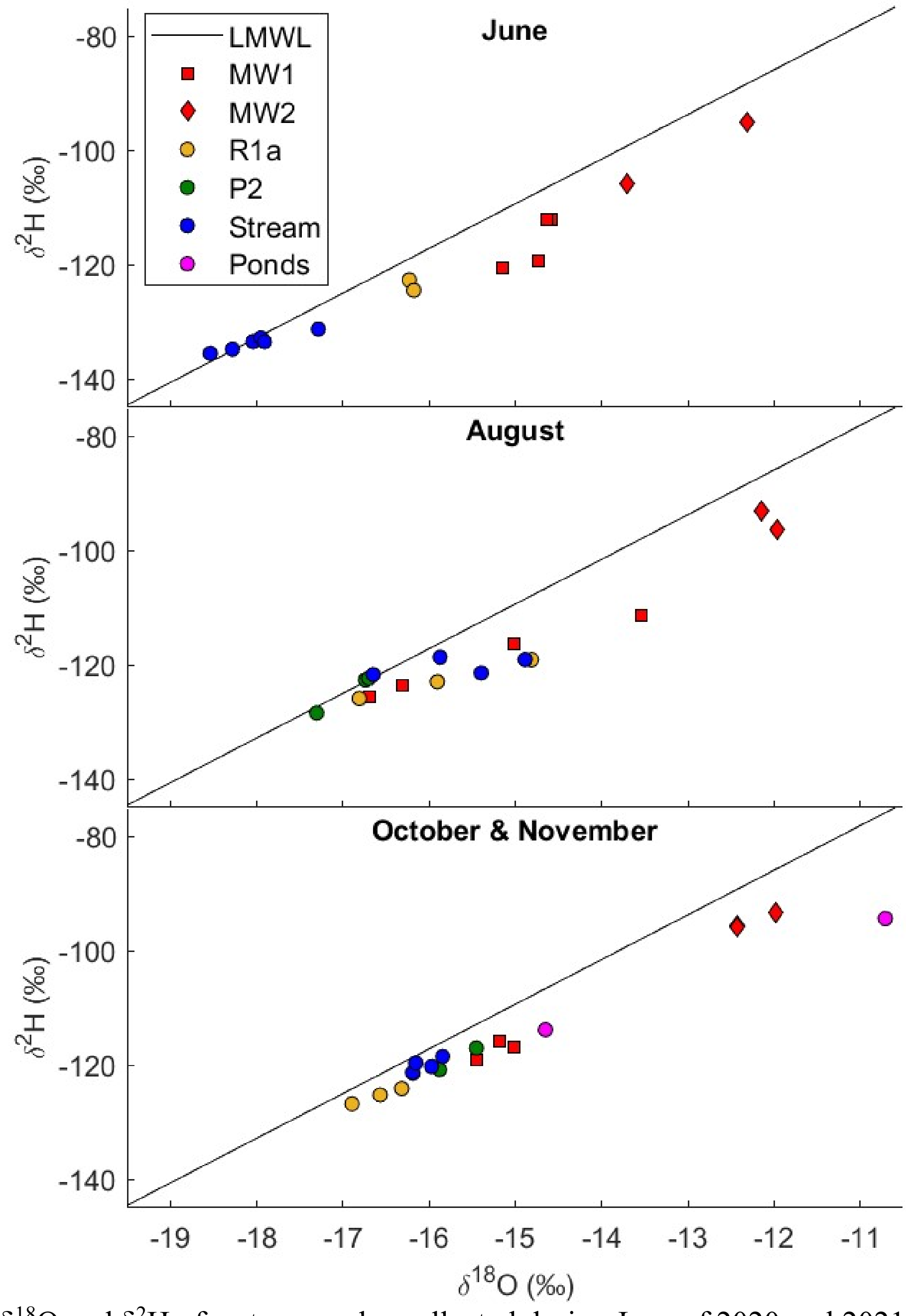

Figure 7: $\delta^{18}O$ and $\delta^{2}H$ of water samples collected during June of 2020 and 2021 (top), August of 2020 and 2021 (middle), and during November 2020 and October 2021 (bottom).

4.2.2 Riparian Well Water

Riparian well water has less temporal variation than stream water but still had noticeable changes in its isotopic composition from month to month. The riparian well water's temporal pattern looks like a muted version of the stream water's pattern; it reaches peak heaviness during August in 2020 and September in 2021 (Figures A3 and A8) before becoming more depleted again during the final sampling event each year (Figures A4 and A9). Riparian well water is isotopically heavier than stream water in the early season (Figures A1, A2, A5 and A6) and becomes isotopically lighter than stream water by the fall. By October and November, riparian well water becomes the most depleted source water (Figures A4 and A9). Riparian well water always falls below the LMWL, indicating some evaporative effects. This is most pronounced in August 2020 and September 2021 (Figures A3 and A8), the same times that the riparian well water was isotopically heaviest.

4.2.3 Piezometer Water

At the downstream station, samples were collected from the deeper of the two nested piezometers, which is slotted at an approximate depth of 1 m below the streambed. Piezometer samples were not collected in June when the stream was too high to wade. Piezometer water shows seasonal variation, typically with similar values to stream water, but slightly delayed. Often, piezometer water has a similar isotopic composition to stream water from the month before. This is especially clear in Figures A2 and A3, Figures A6 and A7, and Figures A8 and A9. Piezometer water plots on or slightly below the LMWL, indicating some mild evaporative effects.

4.2.4 MW1 Water

Of the two deep wells, MW1 shows more seasonal variation (Figure 7). In contrast with the stream and riparian wells, MW1 water is isotopically heaviest in early summer and becomes more depleted throughout the summer. In 2020, MW1 water is isotopically heaviest in June and then is much more depleted through early fall (Figures A1 – A4). In 2021, MW1 shows a similar pattern to 2020, but becomes slightly heavier again in October (Figure A9). MW1 water is isotopically heavier than stream and riparian well water in early summer (Figures A1 and A5) but becomes more similar to stream and riparian well water by later summer and early fall (Figures A4 and A7). MW1 water always plots below the LMWL, indicating some evaporative effects. There were no clear temporal patterns in MW1 water's position relative to the LMWL.

4.2.5 MW2 Water

By far, the isotopically heaviest groundwater samples come from MW2 (Figure 7). MW2 water has very little seasonal variation and remains isotopically heavier than stream water or any other well water in every month. MW2 water is very isotopically similar to water from one of the two sampled ponds. MW2 water always plots well below the LMWL, indicating strong evaporative effects.

4.2.6 Pond Water

Surface water samples were collected from two moraine ponds on the southeast side of the valley (Figure A9) in October 2021 in an attempt to determine the source of the groundwater at MW2. Water from the pond closest to MW2 was some of the isotopically heaviest water collected during this study. This sample is slightly heavier and even further below the LMWL than MW2 water (Figure A9), indicating strong evaporative effects. The other pond samples came from a smaller seasonal pond further upgradient, located between the upstream and downstream monitoring transects. This pond sample was not as isotopically heavy as MW2 water, but still heavier than all other well and stream water samples.

4.3 Flow Modeling Results

4.3.1 Calibration

Model calibration was initially performed using the steady-state model that approximated baseflow conditions during August. Calibration involved trial and error adjustment of hydraulic conductivities, recharge rates, and ET rates, within reasonable ranges determined from field data and/or literature values. Model fit was evaluated by qualitatively examining simulated head contours and comparing observed and simulated head values at the six well locations. Model fit was also evaluated quantitatively by adjusting parameters to minimize the MAE/range ratio (mean absolute error divided by the range in observed head values). The target value for this statistic was < 10%, indicating that the average error magnitude is small relative to the observed range in heads. Final calibrated parameter values and other model inputs are reported in Table 3.

Calibrated hydraulic conductivities range from 0.02 to 10 m/d. The highest hydraulic conductivity of 10 m/d was implemented in the upper model layer in the terrace area. This value is within the range measured during specific capacity tests (Section 4.1.3). The floodplain in the upper layer had a slightly lower hydraulic conductivity of 8 m/d. The till had the lowest hydraulic conductivity in the upper layer, of 2 m/d. Modeled hydraulic conductivity values in the lower layer were generally less than values in the upper layer. In the lower layer, the calibrated hydraulic conductivity was 4 m/d beneath the floodplain and terraces, and 0.02 m/d elsewhere.

Table 3: Model parameters.

Parameter	**Value(s)**
Hydraulic conductivity [m/d] *	0.02 - 10
ET – riparian area [m/d] **	0 - 0.02
Recharge – moraines [m/d]	0.0003
Recharge – floodplain/terrace [m/d]	0.00005
Flow into first stream cell [m^3/d] ***	7,341 -176,433
Streambed conductivity [m/d]	15
Stream width [m]	7
Streambed thickness [m]	1
GHB conductance [m^2/d]	10
GHB distance [m]	400
Constant head - lower pond [m]	2,760
Constant head - upper pond [m]	2,763
Specific storage [m^{-1}]	0.0008
Specific yield	0.15
Effective porosity	0.15
Manning's roughness	0.035

Notes:
*Refer to Figures 3 and 4 for a map of the hydraulic conductivity zones. **Modeled ET is highest during the summer months. ***Range of (incoming) streamflow values specified in the transient model, based on monthly averages of stream discharge during 2020.

Recharge was calibrated for two zones: one zone that coincided with the floodplain and terrace areas and another zone encompassing the moraines. Calibrated recharge rates in both zones were a relatively small fraction of the average precipitation rate. Calibrated recharge into the moraines was 0.0003 m/d, about 23% of the average daily precipitation. Recharge into the floodplain and terrace was 0.00005 m/d, only about 4% of the daily average precipitation rate.

For the steady-state model, the calibrated ET rate was 0.02 m/d for the floodplain zone that contained phreatophytes (willows). This value was used as the maximum growing season ET rate in the transient model during July and August. Minimum growing season ET values of 0.002 m/d were used for May and October.

4.3.2 Transient Model Results

The transient model was developed to investigate seasonality in groundwater flow and groundwater-surface water interactions. Field data collected during May to October 2020 were used to constrain the model. Monthly average stream discharges from the S1 stream gauge were used to assign incoming streamflow, a required input for the SFR Package (Table 4). The transient model was evaluated by comparing observed and simulated heads, examining stream-aquifer interactions, and qualitatively evaluating the simulated head contours.

Table 4: Monthly average stream discharge at the upstream gauge during May to October 2020.

Month	**Average Discharge [m^3/d]**
May	123,894
June	176,433
July	79,850
August	27,865
September	8,842
October	7,341

The transient model reproduces the seasonal patterns of head increase (May – June) and decrease (July – October) that were recorded at observation wells (Figures 8 and 9). The observed head values used for calibration are reported in Appendix B Table B1. The transient model slightly over predicted some wells and slightly underpredicted others. However, the simulated heads were consistently within 1 m of the observed heads (Figures 8 and 9). The transient calibration resulted in a MAE/Range value of 3.8%, well below the goal of 10% for this ratio. The full suite of calibration statistics for the transient model are summarized in Table 5.

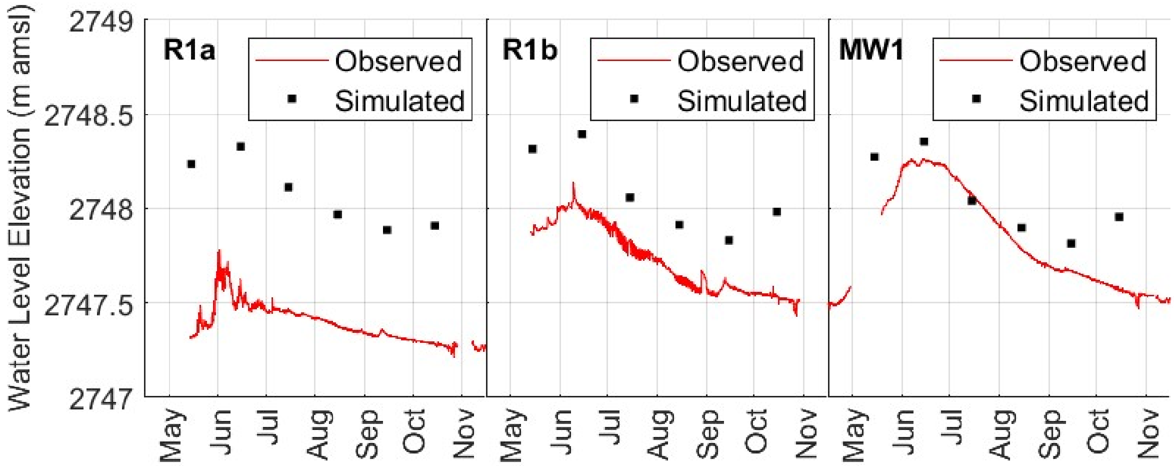

Figure 8: Comparison of observed and simulated heads in upstream wells.

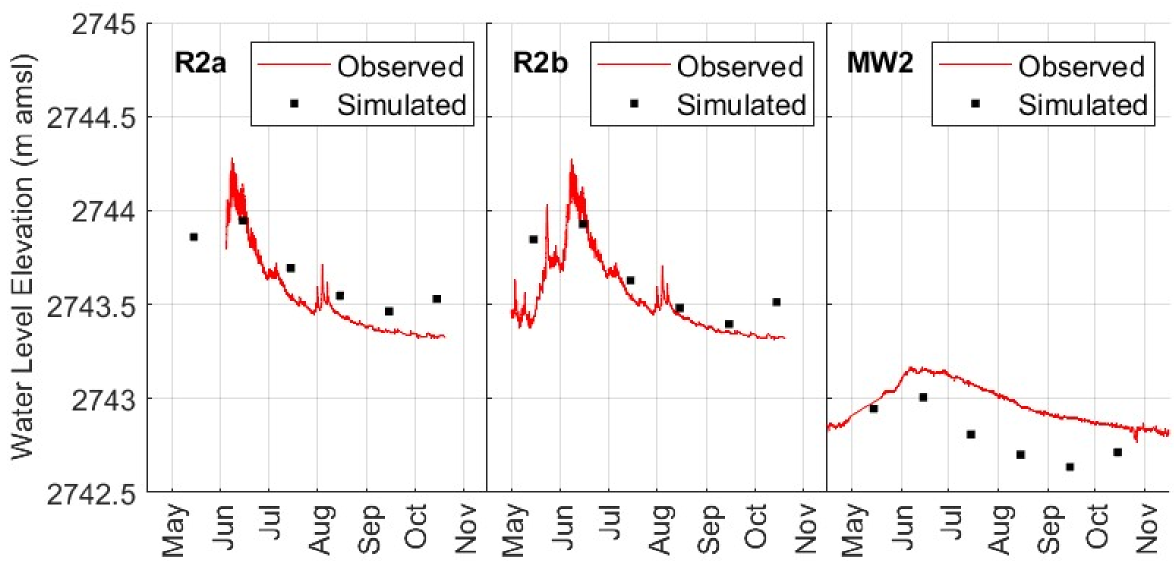

Figure 9: Comparison of observed and simulated heads in downstream wells.

Table 5: Calibration statistics for the transient model. Statistics were calculated using the 35 average hydraulic head values listed in Table B1.

Number of Observations (targets)	35
Mean Error [m]	-0.204
Mean Absolute Error (MAE) [m]	0.272
Root Mean Squared Error [m]	0.349
Range in Observations [m]	5.388
MAE/Range	0.038

Simulated hydraulic head contour maps, included in Figures 10 through 12, help to visualize groundwater flow patterns and directions of groundwater-surface water exchange. Heads were contoured for the last day of each month-long stress period during the six-month simulation. For stress periods representing May and June, the simulated heads indicate strongly gaining stream conditions upstream, and parallel to losing stream conditions downstream (Figure 10). In mid to late summer, the upstream gaining conditions persist, but losing stream conditions are seen further up the valley, especially in July and August (Figure 11). This suggests that the stream recharges the aquifer in mid-late summer. In early fall, conditions gradually transition back to mostly gaining or parallel, similar to early summer (Figure 12). Despite similar contour patterns at the start and end of the transient simulation period, the heads near the stream are lower in early fall than in early summer.

Simulated aquifer inflows and outflows are shown in Figure 13 for June, August, and October. These are global volumetric rates for the entire modeled region. ET and stream leakage change the most from month to month. In June and October, there are more simulated stream gains than stream losses, indicating overall gaining stream conditions during these times. Conversely, in August, there is more leakage out of than into the stream, indicating losing stream conditions. ET outflows are highest in August when maximum ET rates were assumed to occur.

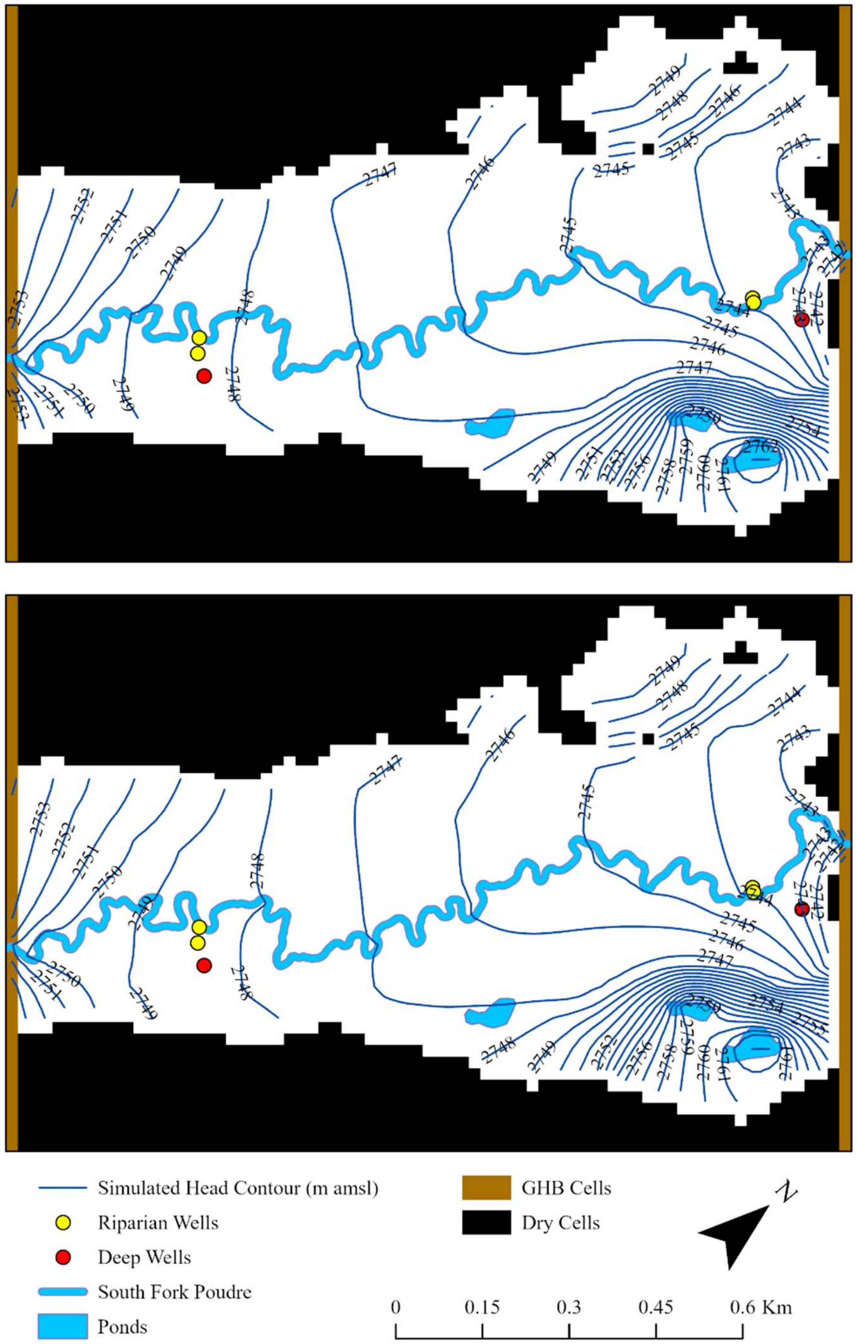

Figure 10: Simulated hydraulic heads in the upper layer during the transient simulation for May (top) and June (bottom).

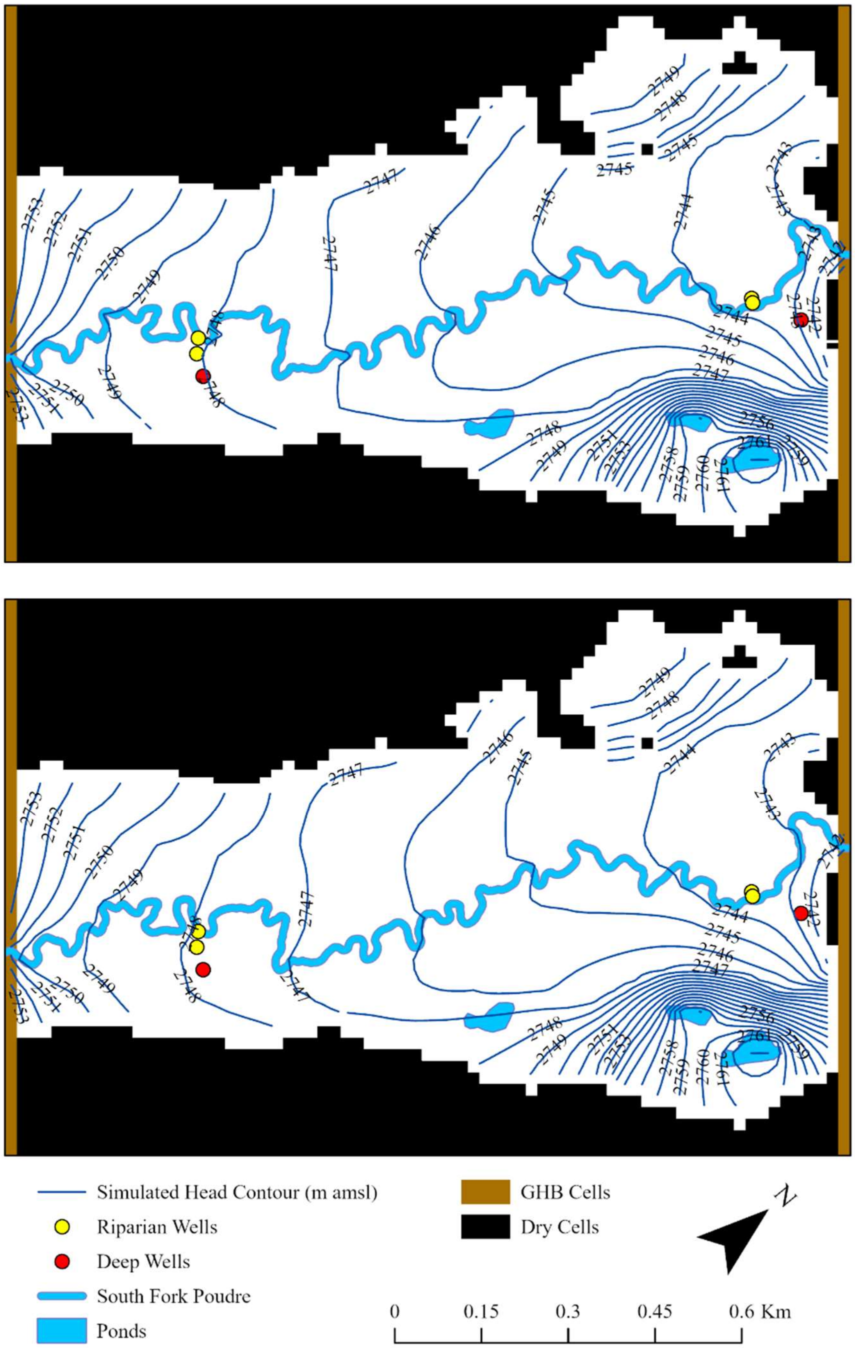

Figure 11: Simulated hydraulic heads in the upper layer during the transient simulation for July (top) and August (bottom).

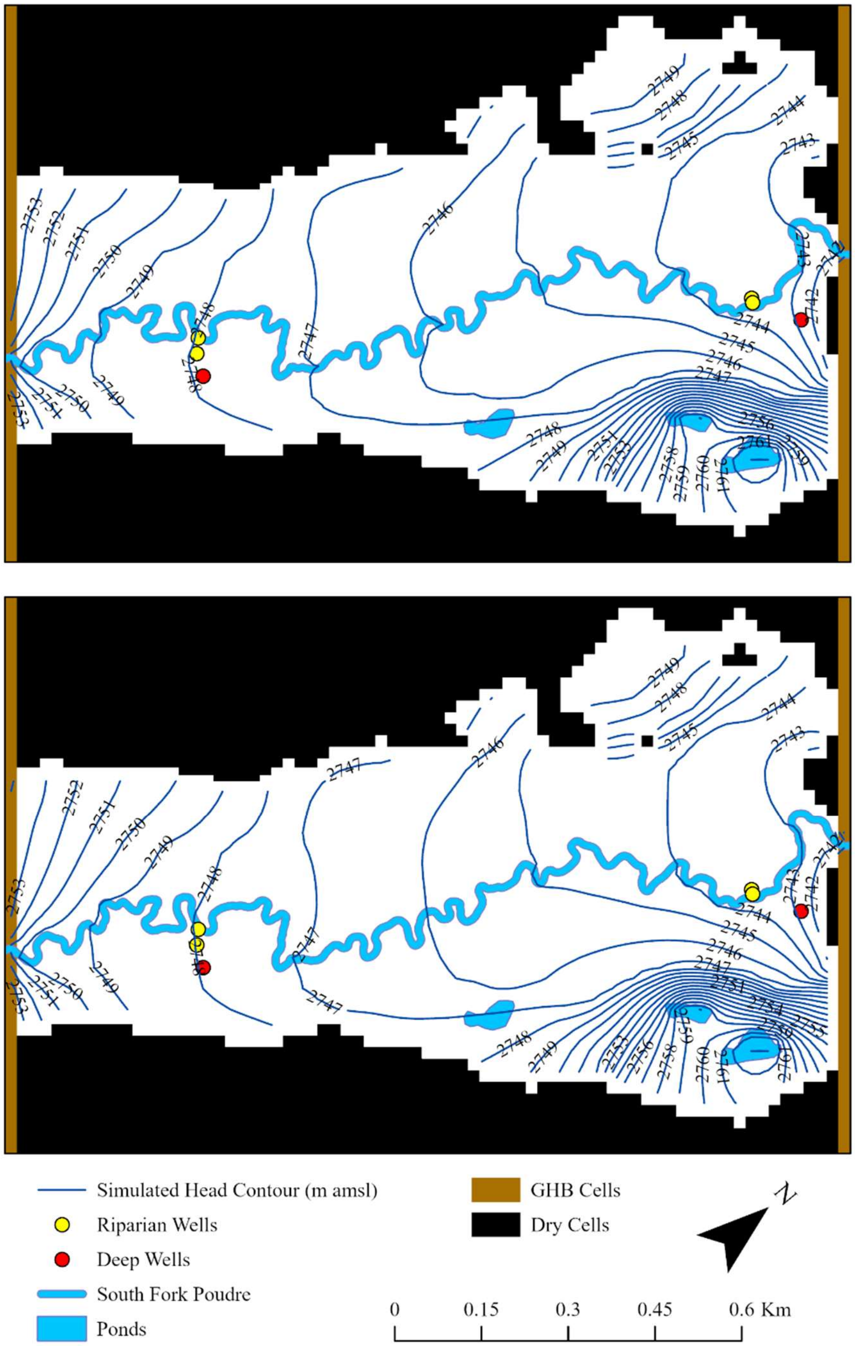

Figure 12: Simulated hydraulic heads in the upper layer during the transient simulation for September (top) and October (bottom).

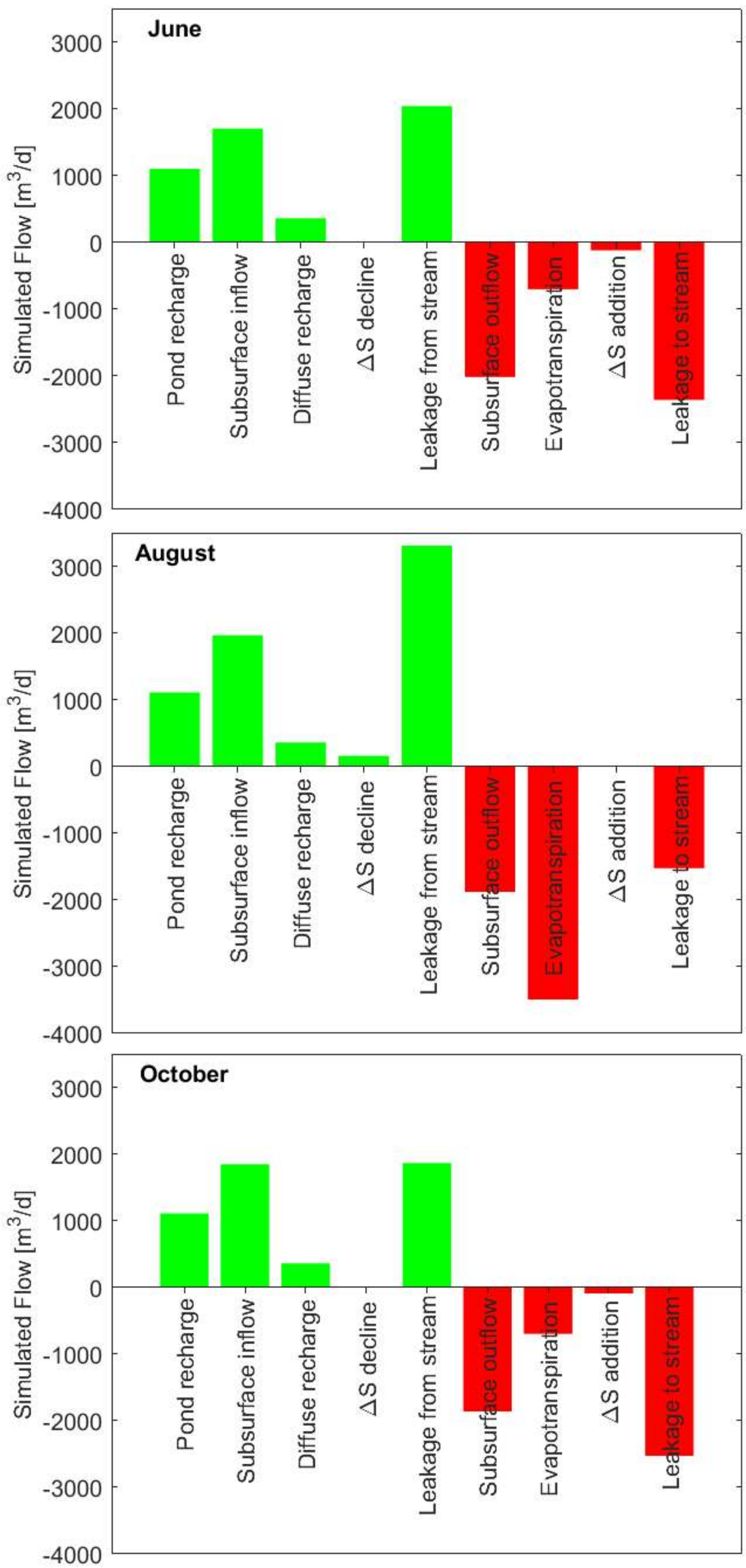

Figure 13: Simulated aquifer water budget for June (top), August (middle), and October (bottom) during the transient simulation. ΔS decline refers to the rate at which water is removed from aquifer storage; ΔS addition refers to the rate at which water is added to aquifer storage.

Simulated streamflow throughout the length of the study reach is illustrated for June, August, and October in Figure 14. Overall, flows are highest in June, lower in August, and lowest in October. Despite their differences in discharge magnitude, June and October have similar spatial flow patterns with distance downstream. During these months, the simulated streamflow increases with distance near the upstream end of the study reach, indicating strongly gaining stream conditions in this area. At intermediate distances downstream, the flow stays roughly constant, alternating between slightly gaining and slightly losing stream conditions. Near the downstream transect, the flow increases slightly with distance again, before abruptly decreasing at the downstream end of the study reach. This indicates a change from weakly gaining to strongly losing stream conditions in the model near the downstream transect.

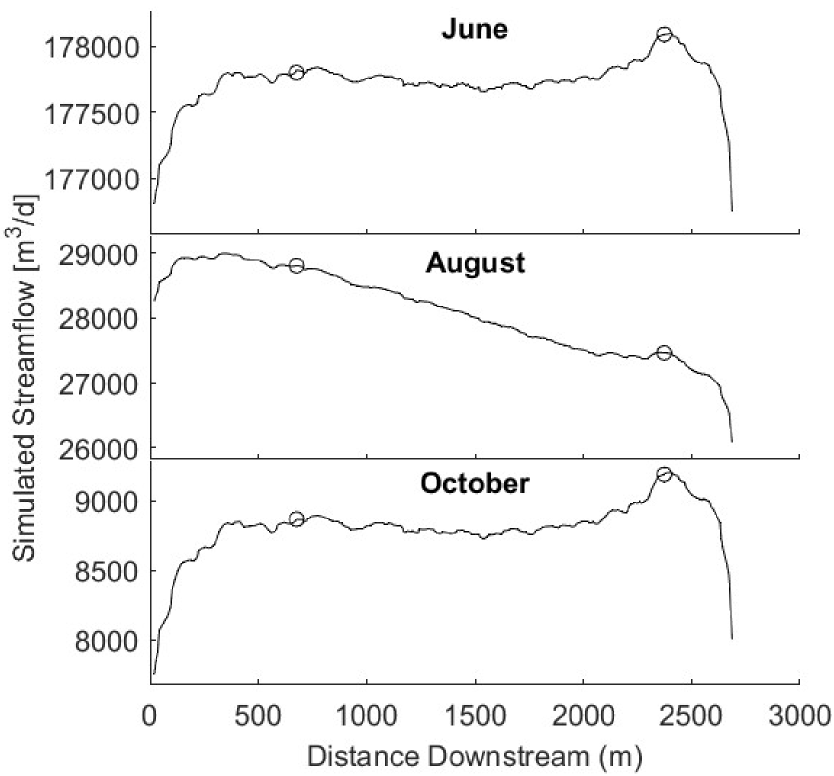

Figure 14: Simulated streamflow versus distance downstream, for June, August, and October. Open circles represent transect locations.

During August, the simulated streamflow patterns are noticeably different from June and October (Figure 14). Gaining stream conditions near the upstream end of the study reach are weaker. The flow continuously decreases with distance through the middle portion of the study reach, indicating losing stream conditions. Closer to the downstream end, losing stream conditions weaken until parallel flow is achieved near the downstream transect. Just past the downstream transect, the channel transitions to strong losing stream conditions.

Notably, some of the strongest gaining and losing stream conditions were observed from stream cells on the model boundary that bordered a GHB cell. At these locations, the magnitude of the simulated groundwater-surface water exchange may be unrealistically high due to artifacts associated with the boundary condition. Importantly, the transect locations where simulated results are evaluated in detail are not directly adjacent to the model boundaries.

The top and middle panels of Figure 15 show the simulated groundwater-surface water exchange throughout the length of the study reach for June and October. During both months, the model simulates gaining stream conditions in the upstream portion of the study reach. Positive flows to the aquifer, indicating losing stream conditions, are found in the downstream portion of the study reach. Overall, both June and October have slightly more negative than positive values for groundwater-surface water exchange, indicating that the stream is overall gaining during these monthly stress periods. This model result is consistent with the results of the streamflow differencing analysis performed using field data (Figure 6).

The bottom panel of Figure 15 shows the difference between June and October simulated groundwater-surface water exchange across the length of the study reach. This graph is included to show the temporal variation in simulated groundwater-surface water exchange, which is not visible in the top two panels of Figure 15 due to the strong spatial variation with distance downstream. The positive values indicate that more stream water enters the aquifer in June than in October, suggesting more stream-sourced aquifer recharge happens earlier in the simulated period.

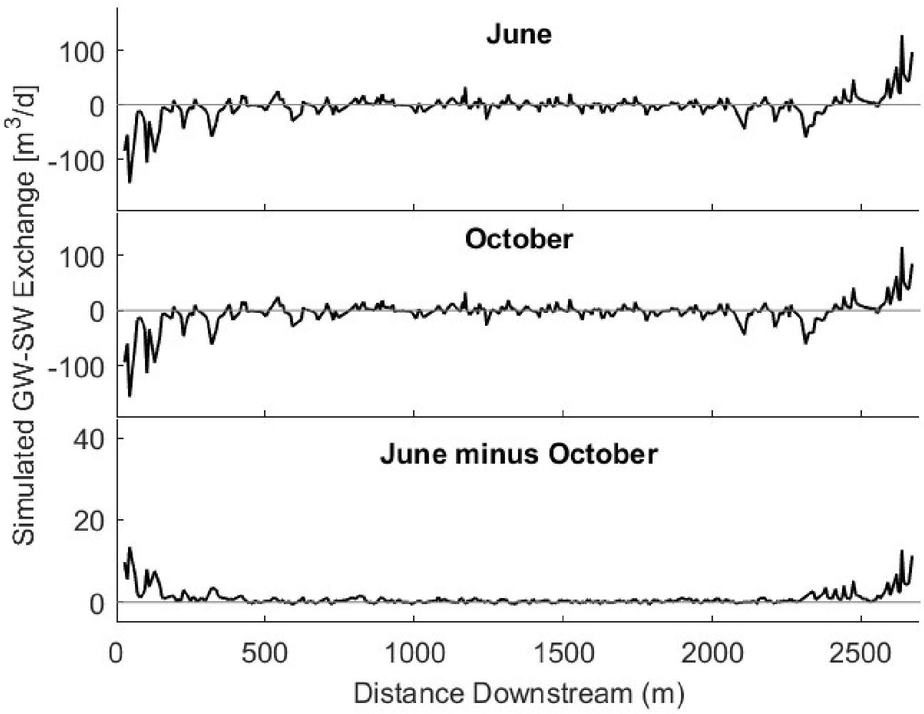

Figure 15: Simulated groundwater-surface water (GW-SW) exchange versus downstream distance in June (top) and October (middle). A positive rate of exchange represents flow into the aquifer (losing stream segment), whereas a negative rate of exchange represents flow out of the aquifer (gaining stream segment). The bottom plot shows the difference between June and October for each stream cell.

4.4 Particle Tracking Results

Simulated reverse flow paths from MW2 indicate that the groundwater sampled at this monitoring well comes from a nearby pond (Figure 16). This pond was not one of the two ponds sampled for isotopes, because it is located on private land. However, this pond is very close to the pond that contained the most isotopically heavy waters. The simulated travel time between the pond and MW2 is ~ 6 months.

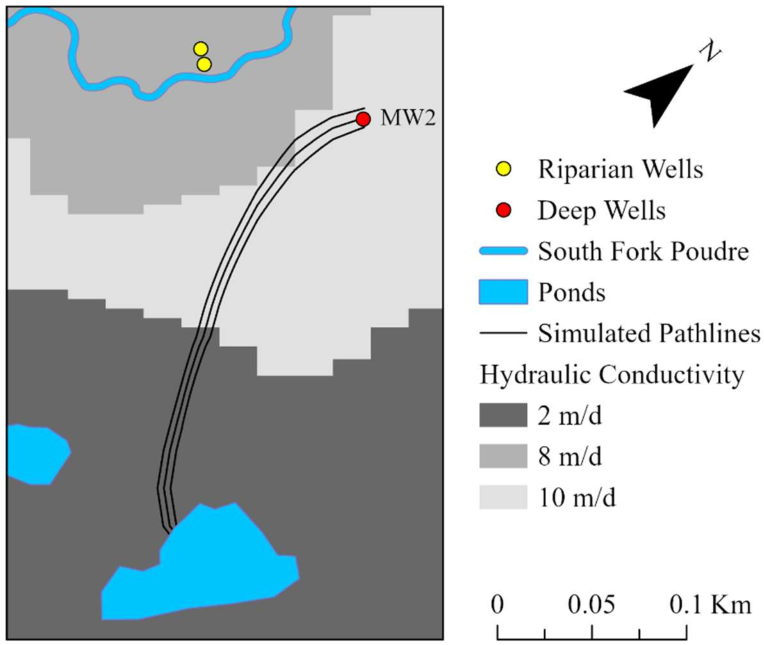

Figure 16: Simulated flow paths from MW2 using reverse particle tracking in the steady-state model.

5. DISCUSSION

This study found that groundwater-surface water exchange at the Mountain Campus is complex, with both gaining and losing stream conditions that vary temporally and spatially along the study reach. This chapter will examine the spatial and temporal variation, sources of aquifer recharge, discuss the suitability of the calibrated model parameters, and end with a note about the Cameron Peak Fire of 2020.

5.1 Spatial Variation in Groundwater-Surface Water Exchange

At the Mountain Campus, groundwater-surface water exchange is spatially variable, a finding that is supported by field measurements at the upstream and downstream transects. A conceptual model for the spatial variation of groundwater-surface water interaction at the Mountain Campus is presented herein, followed by interpretation of the supporting field and model results and a discussion of the mechanisms driving the observed spatial variation.

5.1.1 Conceptual Model

There are both gaining and losing stream reaches along the South Fork within the study area. The most upstream portion of the South Fork near the upstream transect is a gaining reach. The downstream transect has roughly parallel flow on the northwest side of the channel and losing stream conditions on the southeast side of the channel. There is likely a local groundwater divide separating MW2 from the stream at the downstream transect, such that groundwater flows from the moraine towards the divide and also from the stream towards the divide.

5.1.2 Evidence of Spatial Variation

Measured hydraulic heads (Section 4.1.1) support the conceptual model of spatial variation. At the upstream transect, heads decrease closer to the stream, suggesting there is a gradient towards the stream. At the downstream transect, the stream and the two riparian wells on the northwest side of the channel all have nearly identical heads (Figure 5). MW2, on the southeast side of the channel always has a much lower head, which suggests that there could be losing stream conditions on the southeast side of the channel.

Hydraulic heads measured at the piezometer nest indicated losing stream conditions at the downstream transect in most of the months (Section 4.1.1). This is consistent with the conceptual model. However, the piezometer measurements did detect gaining stream conditions one time in August of 2020, which is not consistent with the conceptual model. At this location with nearly parallel flow, there may be short periods of gaining stream conditions, but without pressure transducers installed in the nested piezometers, it is difficult to determine the duration and magnitude of any such periods.

At the upstream transect, groundwater samples collected from well MW1 showed less seasonal variation in isotopic composition than the stream water (Figure 7). One possible explanation for this is that MW1 is a mixture of stream water and groundwater sourced from the moraines. The addition of well-mixed groundwater would dampen the seasonal variations seen in stream water. While it may initially seem like any stream water presence at MW1 suggests losing stream conditions at the upstream transect, this is not necessarily the case. For example, stream water may enter the near-stream portions of the aquifer along meander bends further up the valley. That water may mix with the moraine-sourced waters, then eventually make its way back into the stream at the next meander bend, where gaining stream conditions occur. This is supported by past studies that found evidence of inter-meander bend groundwater flow paths in highly sinuous streams (Wroblicky et al., 1998; Boano et al., 2006).

Isotopic compositions at MW2 are distinct from MW1. MW2 water has very little temporal variation in its isotopic composition and is noticeably heavier than stream water (Section 4.2). This suggests that very little stream-sourced water reaches MW2, since stream water has significant temporal variation. This inspired us to look for other possible sources of groundwater near MW2; samples for stable isotope analysis were collected at two moraine ponds. The similarities between MW2 and the closest sampled pond suggest that infiltrated pond water is the main source of groundwater at MW2. As groundwater flows from the pond to MW2, it may also mix with a small amount of infiltrated precipitation, causing MW2 water to be slightly more depleted and a little closer to the LMWL, compared to pond water (Figure 7, bottom panel). Additional sampling of pond water on a monthly basis and tracer injections into the pond could help determine the relative proportion of pond-sourced water versus other water at MW2.

Shallow groundwater sampled from the deeper piezometer (~ 1 meter below streambed) often had a similar isotopic composition to the stream water from the month before (e.g., Figures A2 and A3; Figures A6 and A7; Figures A8 and A9). This suggests that the stream is losing at this location (i.e., flow is away from the stream), which is consistent with the hydraulic head data from the wells (Figure 5). Since the results suggest there are different flow directions on either side of MW2, there may be a local water divide separating MW2 from the stream.

Both simulated streamflow and simulated groundwater-surface water exchange show a gaining reach at the upstream end of the model domain and a losing reach at the downstream end (Figures 14 and 15). This can also be seen in the simulated hydraulic head contours (Figure 10 –

12). Gaining stream behavior in the simulated head contours does not appear at the location of the upstream transect in every month but, in general, the upper part of the study reach is gaining in model simulations.

At the downstream transect location, the simulated streamflow and simulated groundwater-surface water exchange suggest there is nearly parallel flow. This is also apparent in the simulated hydraulic head contours, particularly on the northwest side of the channel (Figures 10 – 12). Parallel flow on the channel's northwest side is consistent with hydraulic head data from the stream and riparian wells at the downstream transect. Reverse particle tracking showed a pond as the source of groundwater sampled at MW2, consistent with the conceptual model and the isotopic results. The model simulates losing stream conditions downgradient from the downstream transect.

5.1.3 Mechanisms Driving Spatial Variation

Both field data and modeling supported the conceptual model of spatial variation: the South Fork is generally gaining in the upstream part of the study area and losing in the downstream part. The valley at the Mountain Campus widens downgradient. This represents an increase in the cross-sectional area of aquifer sediments, which can be seen in the geometry of the mapped terrace hydrogeomorphic unit in Figure 2. An increased area generally translates into lower heads and a reduction in the hydraulic gradient; however, this effect may be partially offset by additional groundwater inputs along the flow path. Nonetheless, the widening valley would tend to favor reduced aquifer heads and therefore losing stream conditions in the lower part of the study area, as described in the conceptual model.

Changes in channel planform also affect gaining and losing stream conditions. For example, the upstream transect is on the outside of a highly sinuous meander bend. The outsides of meander bends experience some of the greatest groundwater inflows in gaining streams (Balbarini et al., 2017). In highly sinuous streams, inter-meander bend groundwater flow paths may occur, causing stream water from a losing segment to reenter the stream at the next gaining stream segment (Boano et al., 2006). This sort of complex inter-meander bend behavior may be one source of the groundwater near the upstream transect, in this particularly sinuous part of the channel.

Below the downstream transect, the land surface gradient increases toward the end of the valley. This steepening may increase the hydraulic gradient towards the valley's end (Figure 2). This could promote groundwater flow directly out of the valley rather than towards or away from the channel at the downstream transect, leading to less groundwater-surface water exchange in this location. This steepening may also help produce a local groundwater divide near MW2, such that flow paths originating from the moraine and stream converge and flow towards the end of the valley due to the steep gradient.

5.2 Temporal Variation in Groundwater-Surface Water Exchange

We hypothesized that the relative importance of groundwater contributions to the South Fork would increase throughout the summer and early fall following snowmelt. However, this project's results suggest that the direction of groundwater-surface water exchange changes multiple times between May and October, likely due to multiple driving factors that include seasonality in ET and seasonal changes in surface water contributions. The model and field data support this.

5.2.1 Conceptual Model

Figure 17 diagrams the conceptual model for temporal variation in groundwater-surface water exchange for the entire study reach at the Mountain Campus. This portion of the South Fork is losing water to the aquifer in late May. It rapidly transitions to gaining stream conditions in early June during peak streamflow from snowmelt. The gaining behavior tapers off during late June as growing season ET ramps up. The study reach remains overall losing throughout the mid-summer. Finally, the study reach gradually transitions back to gaining stream conditions in the late summer. At some point between October and May, the conditions must revert to losing, however the exact timing of this switch is beyond the scope of this project, which focused on the period between late spring and early fall.

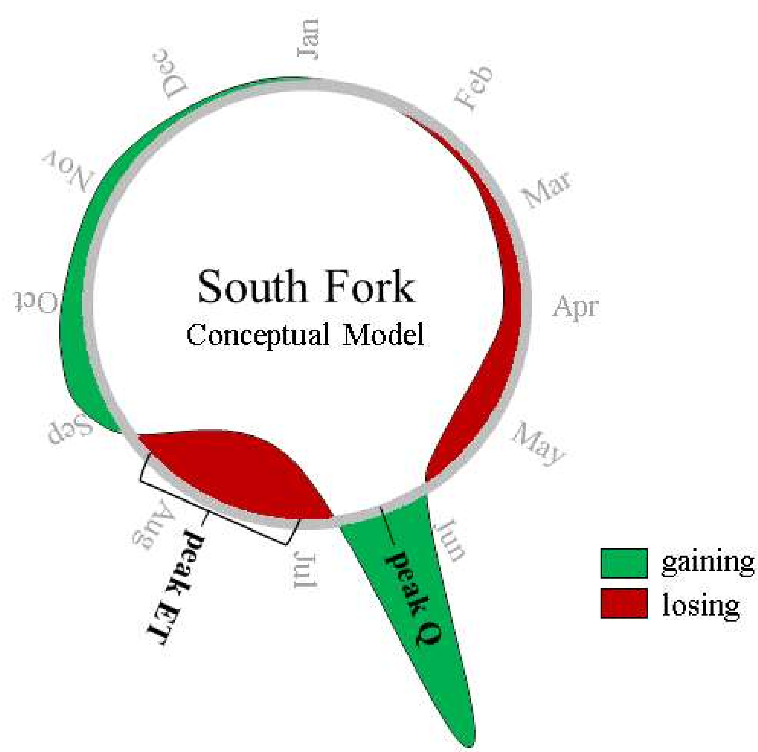

Figure 17: A conceptual model of temporal variation in groundwater-surface water exchange for the study reach. Green represents gaining stream conditions and red represents losing stream conditions. The timing of peak ET and peak discharge (Q) are shown on the diagram.

5.2.2 Evidence of Temporal Variation

Direct field data and numerical modeling both support the conceptual model of transient groundwater-surface water interactions. Field data support of the conceptual model comes from the streamflow differencing results. Losing stream conditions at the end of May rapidly change to the greatest gaining stream conditions in early June (Figure 6). Peak gaining stream conditions occurred within a day of peak streamflow during snowmelt in both 2020 and 2021. This suggests that the sudden change to gaining stream conditions is related to the rapid snowmelt and increased surface water inputs. Based on the streamflow differencing analysis, stream conditions shift back to losing in late June and back to gaining again in August. Conditions must change from slightly gaining back to slightly losing (as seen in May) at some point during the colder months (November – April) when the gauges are not instrumented. Both 2020 and 2021 have roughly the same temporal pattern of streamflow difference between upstream and downstream transects, although the magnitude of these differences varies between years (Figure 6).

It is important to note that streamflow differencing comes from two discharge hydrographs generated from rating curves. A rating curve represents an empirically derived relationship between stream water level and stream discharge based on a limited number of discharge measurements. Any error in the rating curves may propagate to the streamflow differencing, affecting the timing of the observed transitions between gaining and losing stream conditions as well as the magnitude of the exchange. This is particularly true for the highest flows, which come from portions of the rating curves with fewer manual measurements. At the Mountain Campus, peak flow occurred in early June. Consequently, the strong gaining stream conditions seen in early June in Figure 6 have the most uncertainty. Error from the rating curves may contribute to the apparent magnitude of the exchange at this time. However, it is worth noting that the numerical model also indicates a gaining stream during June. During the time periods with lower flows, estimated stream discharge at both gauges come from portions of the rating curves constrained with more field measurements. Because of this, there is less uncertainty in the streamflow differencing for the lower flow periods in mid-late summer and early fall shown in Figure 6.

Additionally, some of the other field data showed temporal variations. Surface waters become isotopically heavier during the mid-summer. This could be due to temporal variation in the relative role of different stream contributions, or due to temperature's effects on precipitation-sourced contributions. For example, warm-weather precipitation is relatively heavier than cool-weather precipitation (Clark & Fritz, 1997). Temporal variation in well water isotopic composition is difficult to interpret because travel times from groundwater sources to the wells are unknown.

Temporal variation of groundwater-surface water exchange is clear in the modeling results. The simulated water budget shows that simulated stream leakage to the aquifer is highest in August (Figure 13). Simulated streamflow also shows an increase in the proportion of the study reach with losing stream conditions at this time (Figure 14). Both of these results support the conceptual model. Simulated hydraulic head contours in Figure 10 also show an overall higher hydraulic head throughout the aquifer in June than May, as seen in the water level elevation data. This suggests that higher surface water inputs into the first stream cell are effective at increasing heads throughout the aquifer, inducing gaining stream conditions. This is followed by a decrease in simulated hydraulic heads in the mid-summer, especially in the near-stream areas where there is an increase in modeled ET (Figure 11). In September and October, the hydraulic heads recover slightly (Figure 12), during the time that modeled ET is tapered off.

These findings suggest that ET plays an important role in lowering the near-stream heads and inducing losing stream conditions in the mid-summer.

5.2.3 Mechanisms Driving Temporal Variation

We propose that seasonal changes in surface water inputs (i.e., incoming streamflow) and ET are the primary mechanisms driving temporal variations in groundwater-surface water exchange. The timing of the gaining and losing stream conditions provides insight into the likely driving mechanisms. Field data indicate that the time period in June with the highest stream discharge aligns with the timing of peak gaining stream conditions. We also noticed that mid-summer losing conditions occur during the period that willows have fully developed leaves, and the days are longest. We suspect that during this period ET is great enough to lower the hydraulic heads near the stream and induce temporary losing stream conditions.

Towards the end of summer, ET starts decreasing as the willow leaves begin to senesce in preparation for winter dormancy and the days become shorter. As ET tapers off, the near-stream hydraulic heads may recover slightly throughout September and October, once again creating a gradient towards the stream, inducing gaining stream conditions. At some point over the winter, the stream slowly shifts back to losing stream conditions, as seen in May. This suggests that supplying baseflow to the stream gradually lowers aquifer heads throughout the winter, eventually reversing the gradient.

5.3 Recharge Sources for the Aquifer

We evaluated the field and model results to determine the relative importance of each source of aquifer recharge. We suspect stream leakage and pond leakage are the most important aquifer inflows. Precipitation-sourced diffuse recharge along moraines is not well characterized, but it appears to contribute less water to the valley aquifer, compared to the leakage from the stream and ponds.

The isotopic similarities between MW2 and the pond (Figure A9) indicate that water from moraine ponds is an important source of aquifer recharge. This is supported by the simulated water budget, which provides some insight into the relative importance of different sources of aquifer recharge in different months (Section 4.3.2). The simulated water budget suggests that stream leakage and pond leakage are both large contributors to aquifer recharge. Simulated stream leakage increases in the mid-summer while pond leakage has far less temporal variability (Figure 13). The finding that surface water bodies are important sources of groundwater in glacial landscapes is consistent with previous research conducted by Roy & Hayashi (2009) and Christensen et al. (2020). Both of those studies found that leakage from surface water bodies supplies a significant groundwater flow path that moves along the surface of the bedrock within moraines.

Within the study area, groundwater is also supplied by subsurface inflow from further upgradient in the valley. This contribution is represented in the model, although the amount and original sources of this groundwater are not well constrained. For example, subsurface inflow could be originally sourced from pond leakage, stream leakage, or diffuse recharge outside of the model domain. For this reason, analysis of the simulated water budget results focuses on the other aquifer inputs that have known original sources within the model domain.

5.4 Model Calibration

Hydraulic conductivities, recharge, and ET rates were calibrated to minimize the differences between simulated and observed hydraulic heads at well locations. In general, the model calibration resulted in parameter values within expected ranges based on field data and literature values.

5.4.1 Hydraulic Conductivity Values

The modeled hydraulic conductivity zone locations in the upper layer came directly from the hydrogeomorphic map from Suhr (2021). Most of the calibrated hydraulic conductivity values for each zone fall within the range of measured field values from the Mountain Campus site or values from other literature in nearby areas. The hydraulic conductivity value for till in the upper layer was 2 m/d. This falls in the middle of the range of alpine glacial till hydraulic conductivities measured at the Glacier Lakes Ecosystem Experiments Site, located roughly 100 km from the Mountain Campus (Ronayne et al., 2012). Within the terrace and floodplain areas, the upper layer calibrated hydraulic conductivity values were 10 m/d and 8 m/d, respectively. Both of these values fall between the aquifer hydraulic conductivities estimated from the specific capacity tests at MW1 and MW2.

The boundary between the upper and lower model layers is a subdued version of the surface topography. This is supported by geophysical surveys of multiple lateral moraines in the Swiss Alps that showed sloping bedrock and internal layering subparallel to the moraine surface (Lukas & Sass, 2011). Compared to the upper layer, lower hydraulic conductivity values were specified beneath the moraines in the lower layer; this is consistent with observations of downward fining within high-elevation deposits (Clow et al., 2003; Sass, 2006). Past studies from the Canadian Rockies found evidence of slow flow paths through fractured bedrock beneath moraines (Roy & Hayashi, 2009; Christensen et al., 2020). Beneath the valley floor, the calibrated hydraulic conductivity value in the lower layer was 4 m/d, which is slightly lower than the hydraulic conductivity value obtained from a specific capacity test at MW1 (4.7 m/d). This could suggest some downward fining of terrace sediments as well.

5.4.2 Recharge Rates

The model included two recharge zones. The calibrated recharge rate on the moraines was 0.0003 m/d, about 23% of the average daily precipitation rate for the period from May to October. Researchers in the Swiss Alps observed very high saturated infiltration rates which prevented infiltration-excess overland flow on moraines of similar age to the ones at the Mountain Campus site (Maier et al., 2020; Maier & van Meerveld, 2021). If the Mountain Campus moraines have similarly high saturated infiltration rates, this could suggest that the diffuse recharge is limited by other factors. For example, in this semi-arid environment, water interception by plant roots in the unsaturated zone may prevent a large portion of infiltrated waters from ever reaching the water table in the moraines. This effect would contribute to the relatively low recharge rate used in the model.

Over the floodplain and terrace, the calibrated recharge rate was 0.00005 m/d, only about 4% of the daily average precipitation rate. The floodplain and terrace likely have lower infiltration rates than the moraines. Suhr (2022) observed a thin, organic-rich surficial layer on the terrace and a fine-grained surficial layer of overbank deposits on the floodplain. Organic and fine-grained surficial layers should both impede infiltration. This supports our use of a low floodplain and terrace recharge value.

Notably, the calibration process revealed that the model was much less sensitive to changes in recharge than changes in other parameters, such as ET rates. This was qualitatively determined by adjusting model recharge values and examining the resulting changes in the simulated hydraulic heads.

5.4.3 Evapotranspiration Rates

The model included ET from the upper model layer in the floodplain where there are dense willows (*Salix sp.*). Willows are deep-rooted phreatophytes that draw water from the saturated zone in areas where the water table is near the surface (Robinson, 1958). No ET was modeled in the terrace and till areas where the vegetation roots likely only draw water from the unsaturated zone, due to the types of vegetation and a greater depth to the water table.

The model included temporal variation of floodplain ET, with no ET from November to April and gradual tapering up and down from the maximum ET value at the start and end of the growing season. This was done because willows at the Mountain Campus lose their leaves for winter. We gradually increased the modeled ET rate in May and June, the time when willows are growing their leaves. In the model, maximum ET took place in July and August because that is the time of the year when the plant leaves are fully formed, and the days are still quite long. By late summer and early fall, the days are becoming shorter and cooler and willow leaves begin to yellow. Consequently, modeled ET tapers off from September to October.

In the floodplain area, the calibrated maximum ET rate was 0.02 m/d for July and August. When accounting for the entire modeled growing season from May to October, the model's average ET rate is approximately 0.01 m/d. The average value falls within the range of mean growing season ET values from a selection of willow studies presented in a review paper by Frédette et al. (2019). However, this value is near the high end of their range and may be too high for willow vegetation at the Mountain Campus site. We found that simulated hydraulic heads were sensitive to the modeled ET parameter value and zonation. This was qualitatively determined by changing the ET value and examining the resulting changes in the simulated hydraulic heads. The relatively high calibrated ET rate was selected because it kept the near-stream portion of the model from producing saturated conditions at the land surface and it helped prevent overprediction of heads at riparian well locations. The specified ET rates also resulted in mid-summer losing stream conditions, as seen in the streamflow differencing results.

5.5 The Cameron Peak Fire

The Cameron Peak Fire was the largest fire in Colorado history, as of present. The fire started on August 13, 2020, near Cameron Pass in north-central Colorado and burned over 84,000 ha in Northern Colorado within and around the watershed of the Cache la Poudre River (Incident Information System, 2021). The damage impacted nearly 1,000 km of streams within the Cache la Poudre River watershed (Coalition for the Poudre River, 2022b). During the fire, ash fell from the sky on CSU's main campus in Fort Collins, Colorado. Smoke from the wildfire could be seen in neighboring states.

On October 9, 2020, the wildfire reached the CSU Mountain Campus. The fire burned conifer forest along the northwest moraine of the study site (Figure 18). The fire also burned areas higher in the South Fork Poudre watershed which contribute to streamflow in the study area. Although the fire burned within a kilometer of instrumentation used in this study, the impacts on this project were minimal. Just two scheduled field visits to the site were not possible during September and October 2020. However, none of the instrumentation was damaged, and the well and surface water transducers continued logging even as the fire burned nearby.

Figure 18: Wildfire smoke rising from the northwest moraine in the study area, viewed from the upstream transect. This photo was taken by Valerie Doebley on November 6, 2020.

6. CONCLUSIONS AND RECOMMENDATIONS

6.1 Summary

The goal of this project was to collect baseline data to characterize the valley hydrogeology and to quantitively characterize groundwater-surface water exchange along the South Fork of the Cache la Poudre River at the Colorado State University Mountain Campus. The study considered how groundwater-surface water exchange along the study reach is dependent on valley hydrogeologic characteristics as well as seasonal processes. The methods employed in this research were a combination of field data collection and numerical modeling. Field techniques included monitoring hydraulic heads in wells and surface waters, measuring the streamflow difference between two stream gauges, and stable isotope sampling. These data helped constrain a transient numerical groundwater model of the study area. Groundwater-surface water exchange along the study reach was qualitatively examined with simulated hydraulic head contours, and quantitively examined using a simulated aquifer water budget, simulated streamflow, and simulated groundwater-surface water exchange.

Measured water levels at the monitoring wells and stream, along with groundwater modeling results, indicate that the South Fork is generally gaining (i.e., groundwater discharges to the stream) around the upstream transect, while the downstream transect has parallel flow on one side and losing stream conditions on the other side. Isotope and model results suggest that groundwater moves from moraine ponds towards MW2, providing evidence of a local groundwater divide at this location. We suggest that valley geometry and planform influence the spatial differences in groundwater-surface water exchange along the study reach.

Streamflow differencing showed that the study reach switched from overall gaining to overall losing stream conditions multiple times during the period from May to October. We propose that ET and seasonal changes in surface water inputs are the forces driving shifts from gaining to losing stream conditions. Currently, seasonal changes in surface-water contributions are driven by seasonal meteorological shifts, for example, the annual cycle of winter snow accumulation and spring snowmelt. However, climate change could produce similar shifts on a much longer time scale, for example, multiple consecutive years with low snowpack. Furthermore, the simulated water budget indicated that stream and pond leakage are key sources of aquifer recharge at this site. Ultimately, the same climatic trends that impact surface water contributions to streamflow will also impact groundwater contributions because surface water is the main source of groundwater at this site. The point at which we see this impact may be delayed, due to the relatively slower movement of water through the subsurface. However, long-term impacts to groundwater storage are likely to affect the amount and timing of streamflow in mountain watersheds.

6.2 Recommendations for Future Work

The recent instrumentation of the Mountain Campus site benefited this project and will surely provide many future opportunities for research focused on mountain watershed hydrogeology. The results of this project highlight additional areas for future research, including the following: (1) research that investigates wildfire impacts to surface and groundwater resources in the valley; (2) further assessment of riparian zone ET and its impact on groundwater-surface water interaction; and (3) work on the hydrogeologic role of hillslope moraines.

6.2.1 Impacts of Wildfire

Since well monitoring started prior to the Cameron Peak Fire, the Mountain Campus could be an excellent place to study the impacts of wildfire on groundwater and surface water in the future. Furthermore, because the fire burned only one of the two lateral moraines bordering the valley segment, this site could be an interesting set up for a side-by-side comparison of fire's impact on groundwater flow through the two moraines.

Wildfires can produce hydrophobic soils (Robichaud, 2000; Benavides-Solorio & MacDonald, 2001). This could impact diffuse recharge into the burned northwest moraine. However, based on simulated water budgets (Figure 13), diffuse recharge may be a relatively minor source of groundwater compared to the larger aquifer inflows from stream and pond leakage. Consequently, it is possible that the fire's impacts to this aquifer will be relatively small, but more studies are needed to determine if this is the case.

6.2.2 Evapotranspiration Effects

Groundwater modeling performed as part of this study indicates that seasonal changes in ET help drive the temporal variations in groundwater-surface water exchange. Modeled ET values are from calibration rather than field measurement, and the timing of ET tapering is primarily based on qualitative observations of willow leaves. Quantitative studies on willow ET at this site could help to further refine the values and timing of ET. This could be done by examining the existing dataset at riparian zone monitoring wells (water levels recorded at sub-hourly frequency) and applying an analytical solution that solves for groundwater consumption by phreatophytes, such as the White method (White, 1932; Loheide et al., 2005). Willow ET at the Mountain Campus could also be estimated from in-situ measurements, by applying methods like those from the willow ET studies reviewed in Frédette et al. (2019).

6.2.3 Moraine Hydrogeology

Interest in the hydrogeology of glacial deposits rose throughout the last few decades, due to increased scientific awareness of important groundwater contributions to streamflow from coarse geologic units at high-elevation sites (Clow et al., 2003; Williams et al., 2015). Studies from the Lake O'Hara Watershed site in the Canadian Rockies detected three distinct flow paths through moraines as well as hydrogeological mechanisms separating these flow paths (Roy & Hayashi, 2009; McClymont, et al., 2011). These same studies found that lake-sourced water flowing over the surface of the bedrock was the dominant groundwater flow path through the Lake O'Hara moraine. Results from the Mountain Campus suggest that surface water bodies are an important groundwater source at this site as well. This project was limited to a single round of isotopic sampling at two moraine ponds, but even so, isotopic similarities between pond water and groundwater sampled at well MW2 suggest similarities between the Mountain Campus site and the Lake O'Hara Watershed site. Additional pond isotope sampling and level monitoring, in addition to geophysical surveys could provide further insights into the moraine hydrogeology (e.g., flow paths) at the Mountain Campus. Tracer injections into the moraine ponds could also shed light on moraine hydrogeological processes. Particle tracking estimated a ~6-month travel time from the moraine pond to MW2. By injecting a tracer into the pond then watching for the tracer's arrival at MW2, we could determine the actual travel time. Furthermore, by using a method similar to Langston et al. (2013), pond tracer injections could help estimate the hydraulic conductivity value of till on a large scale. Measuring larger scale hydraulic conductivity at this site could help to further refine the hydraulic conductivity values used in numerical modeling.

In addition to tracers, geophysical surveys on the moraines could provide useful information on subsurface structure and water table depth. New data collected on the moraines and elsewhere should be used to update and/or expand the numerical model. The model was created with the hopes that it will be built upon and improved over the years to come and will serve as a useful tool to support continued hydrogeologic research at the Mountain Campus.

REFERENCES

Arnoux, M., Halloran, L. J., Berdat, E., & Hunkeler, D. (2020). Characterizing seasonal groundwater storage in alpine catchments using time-lapse gravimetry, water stable isotopes and water balance methods. Hydrological Processes, 34(22), 4319-4333.

Balbarini, N., Boon, W. M., Nicolajsen, E., Nordbotten, J. M., Bjerg, P. L., & Binning, P. J. (2017). A 3-D numerical model of the influence of meanders on groundwater discharge to a gaining stream in an unconfined sandy aquifer. Journal of Hydrology, 552, 168-181.

Barnett, T. P., Adam, J. C., & Lettenmaier, D. P. (2005). Potential impacts of a warming climate on water availability in snow-dominated regions. Nature, 438(7066), 303-309.

Benavides-Solorio, J., & MacDonald, L. H. (2001). Post-fire runoff and erosion from simulated rainfall on small plots, Colorado Front Range. Hydrological Processes, 15(15), 2931-2952.

Boano, F., Camporeale, C., Revelli, R., & Ridolfi, L. (2006). Sinuosity-driven hyporheic exchange in meandering rivers. Geophysical Research Letters, 33(18).

Caballero, Y., Jomelli, V., Chevallier, P., & Ribstein, P. (2002). Hydrological characteristics of slope deposits in high tropical mountains (Cordillera Real, Bolivia). Catena, 47(2), 101-116.

Campbell, D. H., Clow, D. W., Ingersoll, G. P., Mast, M. A., Spahr, N. E., & Turk, J. T. (1995). Processes controlling the chemistry of two snowmelt-dominated streams in the Rocky Mountains. Water Resources Research, 31(11), 2811-2821.

Chow, V. T. (1959). Open-channel hydraulics. McGraw-Hill civil engineering series. Retrieved from Forest Science Labs. Oregon State University. Available: http://www.fsl.orst.edu/geowater/FX3/help/8_Hydraulic_Reference/Mannings_n_Tables.htm

Christensen, C. W., Hayashi, M., & Bentley, L. R. (2020). Hydrogeological characterization of an alpine aquifer system in the Canadian Rocky Mountains. Hydrogeology journal, 28(5), 1871-1890.

Clark, I. D., & Fritz, P. (1997). Environmental isotopes in hydrogeology. CRC press.

Clow, D. W., Schrott, L., Webb, R., Campbell, D. H., Torizzo, A., & Dornblaser, M. (2003). Ground water occurrence and contributions to streamflow in an alpine catchment, Colorado Front Range. Groundwater, 41(7), 937-950.

Coalition for the Poudre River (2022a). Cache la Poudre Watershed. Available: https://www.poudrewatershed.org/cache-la-poudre-watershed

Coalition for the Poudre River (2022b). Cameron Peak Fire. Available: https://www.poudrewatershed.org/cameronpeakfire

Collins, J. A., & Sprague, L. A. (2005). The Cache la Poudre River, Colorado, as a drinking-water source. US Department of the Interior, US Geological Survey.

Colorado State University (2022a). Mountain Campus Instrumentation Data. Main Weather Station [Unpublished raw data]. Retrieved from CSU Warner College of Natural Resources online. Available: https://datavis.warnercnr.colostate.edu/instrumentation/station_data.cfm

Colorado State University (2022b). History. CSU Mountain Campus. Available: https://mountaincampus.colostate.edu/about/history/

Dassargues, A. (2019). Hydrogeology: Groundwater science and engineering. CRC Press.

Fetter, C. W. (2001). Applied hydrogeology (4th Edition). Waveland Press.

Frédette, C., Labrecque, M., Comeau, Y., & Brisson, J. (2019). Willows for environmental projects: A literature review of results on evapotranspiration rate and its driving factors across the genus Salix. Journal of Environmental Management, 246, 526-537.

Frisbee, M. D., Phillips, F. M., Campbell, A. R., Liu, F., & Sanchez, S. A. (2011). Streamflow generation in a large, alpine watershed in the southern Rocky Mountains of Colorado: Is streamflow generation simply the aggregation of hillslope runoff responses?. Water Resources Research, 47(6).

Harbaugh, A. W. (2005). MODFLOW-2005, the US Geological Survey modular ground-water model: the ground-water flow process. Reston, VA: US Department of the Interior, US Geological Survey. 6-A16.

Harrington, J. S., Mozil, A., Hayashi, M., & Bentley, L. R. (2018). Groundwater flow and storage processes in an inactive rock glacier. Hydrological Processes, 32(20), 3070-3088.

Hood, J. L., Roy, J. W., & Hayashi, M. (2006). Importance of groundwater in the water balance of an alpine headwater lake. Geophysical Research Letters, 33(13).

Incident Information System (2021). Cameron Peak Fire. National Wildfire Coordinating Group. Available: https://inciweb.nwcg.gov/incident/6964/

Landon, M. K., Rus, D. L., & Harvey, F. E. (2001). Comparison of instream methods for measuring hydraulic conductivity in sandy streambeds. Groundwater, 39(6), 870-885.

Langston, G., Hayashi, M., & Roy, J. W. (2013). Quantifying groundwater-surface interactions in a proglacial moraine using heat and solute tracers. Water Resources Research, 49(9), 5411-5426.

Liu, F., Williams, M. W., & Caine, N. (2004). Source waters and flow paths in an alpine catchment, Colorado Front Range, United States. Water Resources Research, 40(9).

Loheide, S. P., Butler Jr, J. J., & Gorelick, S. M. (2005). Estimation of groundwater consumption by phreatophytes using diurnal water table fluctuations: A saturated-unsaturated flow assessment. Water resources research, 41(7).

Lukas, S., & Sass, O. (2011). The formation of Alpine lateral moraines inferred from sedimentology and radar reflection patterns: a case study from Gornergletscher, Switzerland. Geological Society, London, Special Publications, 354(1), 77-92.

Madole, R. F., VanSistine, D. P., & Michael, J. A. (1998). Pleistocene glaciation in the upper Platte River drainage basin, Colorado. US Geological Survey, Geologic Investigations Series, I-2644, scale 1: 300,000.

Maier, F., van Meerveld, I., Greinwald, K., Gebauer, T., Lustenberger, F., Hartmann, A., & Musso, A. (2020). Effects of soil and vegetation development on surface hydrological properties of moraines in the Swiss Alps. Catena, 187, 104353.

Maier, F., & van Meerveld, I. (2021). Long-Term Changes in Runoff Generation Mechanisms for Two Proglacial Areas in the Swiss Alps I: Overland Flow. Water Resources Research, 57(12).

McClymont, A. F., Roy, J. W., Hayashi, M., Bentley, L. R., Maurer, H., & Langston, G. (2011). Investigating groundwater flow paths within proglacial moraine using multiple geophysical methods. Journal of Hydrology, 399(1-2), 57-69.

Meiman, J. R. & Leavesley, G. H. (1974). Little South Poudre Watershed climate and hydrology, 1961-1971, synopsis. College of Forestry and Natural Resources. Colorado State University.

Messerli, B., Viviroli, D., & Weingartner, R. (2004). Mountains of the world: vulnerable water towers for the 21st century. Ambio, Special Report No. 13, 29-34.

National Oceanic and Atmospheric Administration (2020). Global Historical Climate Network. BEAR LAKE, CO US [Unpublished data]. Retrieved from Climate Data Online. National Centers for Environmental Information.

Nesse, W. D., & Braddock, W. A. (1989). Geologic Map of the Pingree Park Quadrangle, Larimer County, Colorado, 1: 24,000 scale. US Geological Survey Map GQ-1622. US Geological Survey: Reston, VA.

Pollock, D. W. (2012). User guide for MODPATH version 6: a particle tracking model for MODFLOW (p. 58). US Geological Survey: Reston, VA.

Prudic D. E., Konikow L. F., & Banta E. R. (2004). A new stream- flow routing (SFR1) package to simulate stream-aquifer interaction with MODFLOW-2000: US Geological Survey Open-File Report 2004-1042. 104.

Razack, M., & Huntley, D. (1991). Assessing transmissivity from specific capacity in a large and heterogeneous alluvial aquifer. Groundwater, 29(6), 856-861.

Robichaud, P. R. (2000). Fire effects on infiltration rates after prescribed fire in Northern Rocky Mountain forests, USA. Journal of Hydrology, 231, 220-229.

Robinson, T. W. (1958). Phreatophytes. U.S. Geological Survey Water-Supply Paper 1423.

Ronayne, M. J., Houghton, T. B., & Stednick, J. D. (2012). Field characterization of hydraulic conductivity in a heterogeneous alpine glacial till. Journal of hydrology, 458, 103-109.

Roy, J. W., & Hayashi, M. (2009). Multiple, distinct groundwater flow systems of a single moraine–talus feature in an alpine watershed. Journal of Hydrology, 373(1-2), 139-150.

Rumbaugh J. O., & Rumbaugh, D. B. (2020). Groundwater Vistas version 8. Copyright 2000-2020. Environmental Simulations, Inc.

Sass, O. (2006). Determination of the internal structure of alpine talus deposits using different geophysical methods (Lechtaler Alps, Austria). Geomorphology, 80(1-2), 45-58.

Siirila-Woodburn, E. R., Rhoades, A. M., Hatchett, B. J., Huning, L. S., Szinai, J., Tague, C., Nico, P. S., Feldman, D. R., Jones, A. D., Collins, W. D., & Kaatz, L. (2021). A low-to-no snow future and its impacts on water resources in the western United States. Nature Reviews Earth & Environment, 2(11), 800-819.

Suhr, J. C. (2021). Map of Hydrogeomorphic Units along the South Fork Cache la Poudre Valley at the Colorado State University Mountain Campus [Unpublished map]. Department of Geosciences, Colorado State University.

Suhr, J. C. (2022). Post-glacial alluvial valley dynamics of the South Fork Cache La Poudre River Valley at the Colorado State University Mountain Campus [Unpublished master's thesis]. Colorado State University, Fort Collins, Colorado.

US Geological Survey (2015). 3D Elevation Program. USGS LPC CO SoPlatte Lot3 2013 LAS 2015. Retrieved from opentopography.org.

US Geological Survey (2017). Water Quality Samples for the Nation. Data for the following sites: USGS 401716105394601 NADP CO98 AND CO89 LOCH VALE ROCKY MNT NAT PRK, CO [Unpublished raw data]. Retrieved from the National Water Information System.

Viviroli, D., Kummu, M., Meybeck, M., Kallio, M., & Wada, Y. (2020). Increasing dependence of lowland populations on mountain water resources. Nature Sustainability, 3(11), 917-928.

White, W. N. (1932). A method of estimating ground-water supplies based on discharge by plants and evaporation from soil: Results of investigations in Escalante Valley, Utah (Vol. 659). US Government Printing Office.

Williams, M. W., Hood, E., Molotch, N. P., Caine, N., Cowie, R., & Liu, F. (2015). The 'Teflon basin' myth: hydrology and hydrochemistry of a seasonally snow-covered catchment. Plant Ecology & Diversity, 8(5-6), 639-661.

Wroblicky, G. J., Campana, M. E., Valett, H. M., & Dahm, C. N. (1998). Seasonal variation in surface-subsurface water exchange and lateral hyporheic area of two stream-aquifer systems. Water Resources Research, 34(3), 317-328.

APPENDIX A

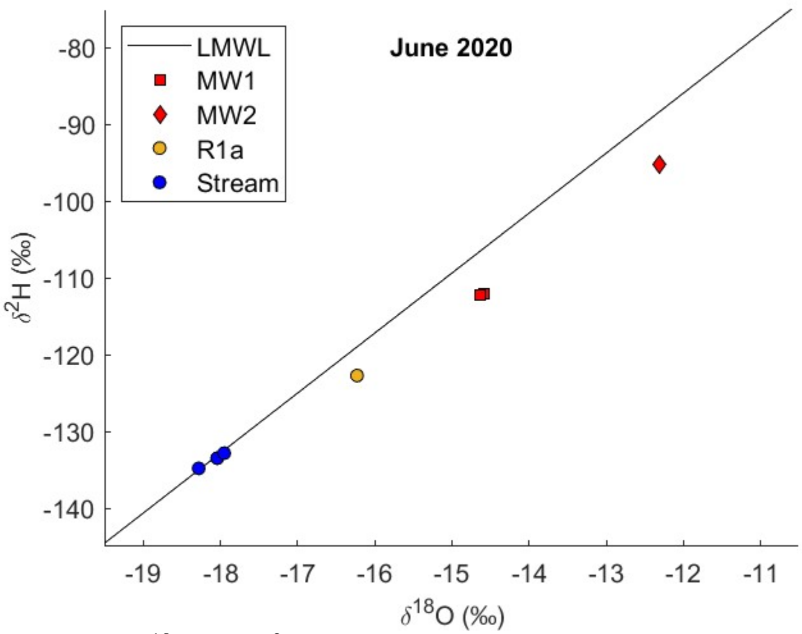

Figure A1: $\delta^{18}O$ and δ^2H of water samples collected during June 2020.

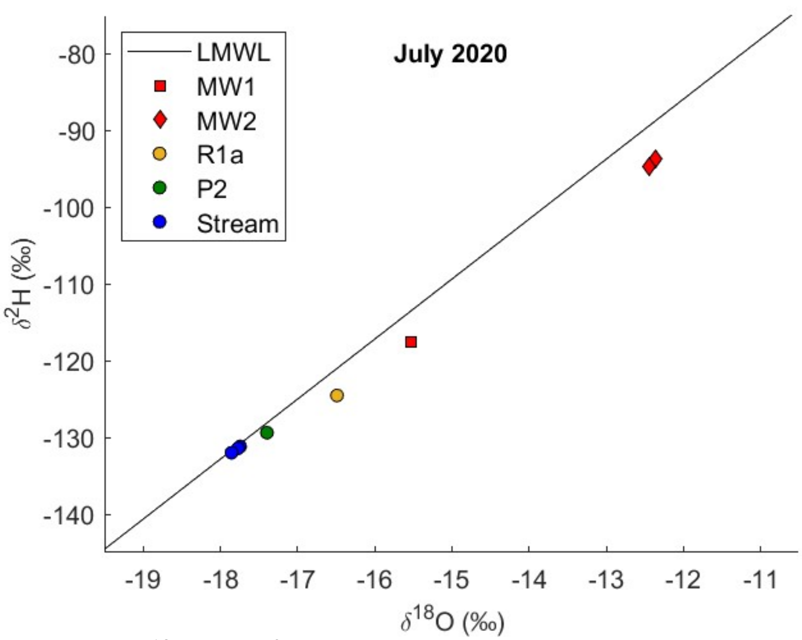

Figure A2: $\delta^{18}O$ and δ^2H of water samples collected during July 2020.

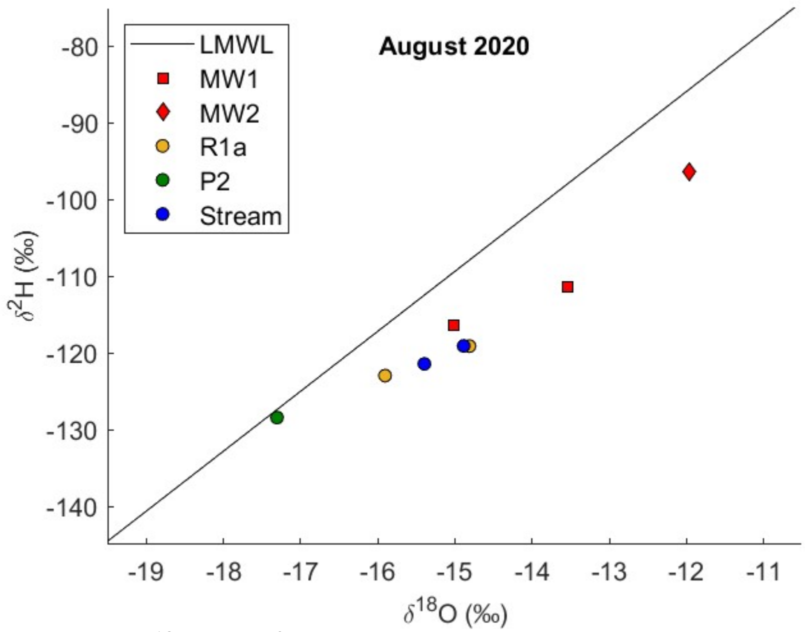

Figure A3: $\delta^{18}O$ and $\delta^{2}H$ of water samples collected during August 2020.

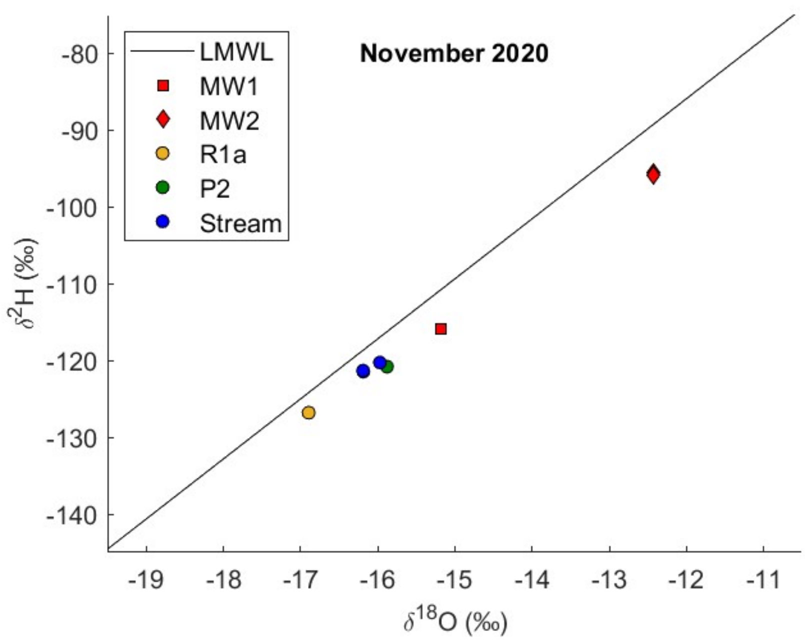

Figure A4: $\delta^{18}O$ and $\delta^{2}H$ of water samples collected during November 2020.

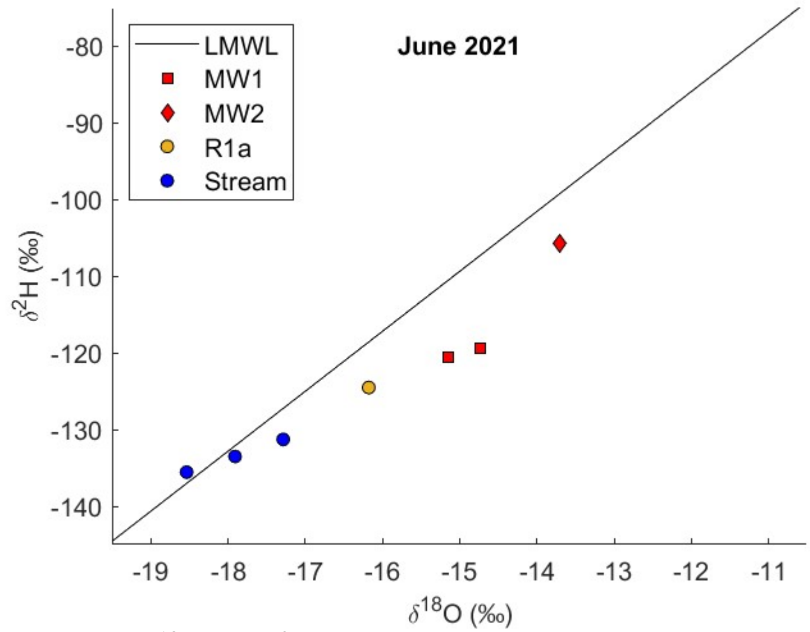

Figure A5: δ^{18}O and δ^2H of water samples collected during June 2021.

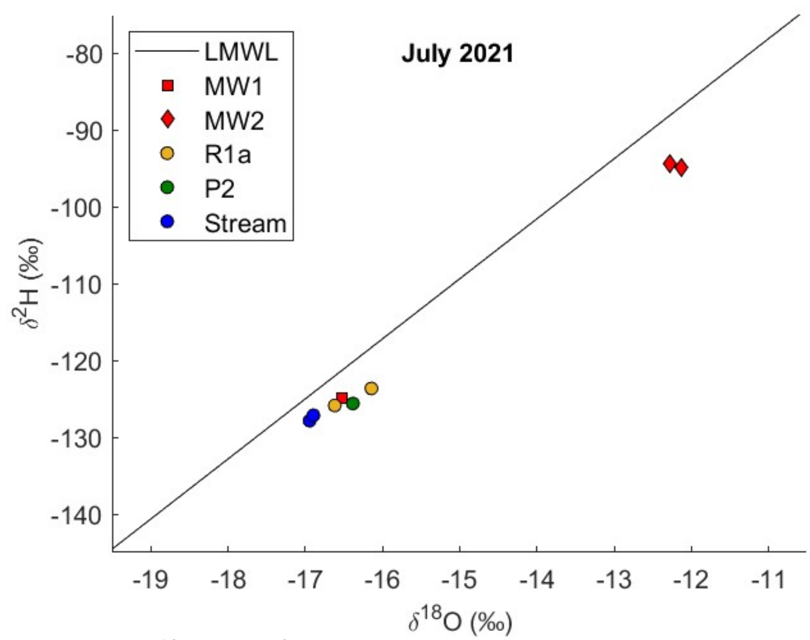

Figure A6: δ^{18}O and δ^2H of water samples collected during July 2021.

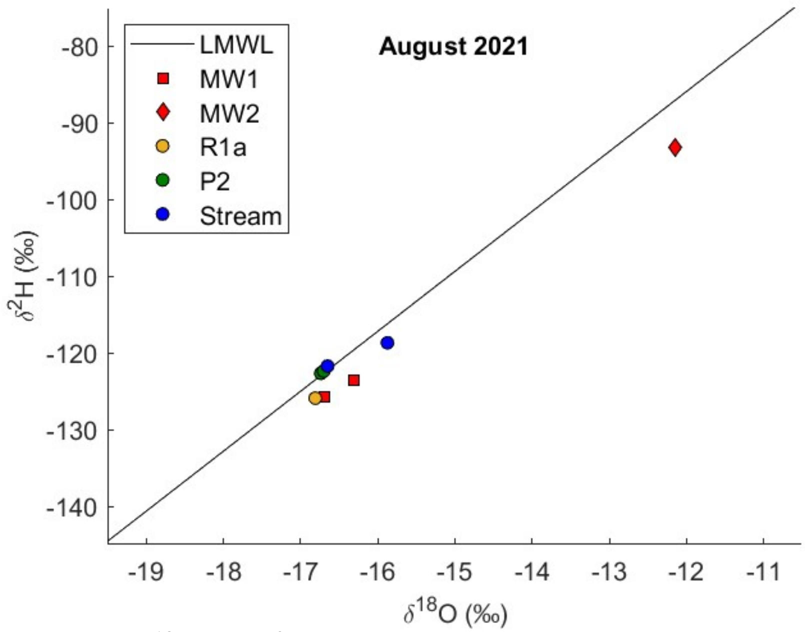

Figure A7: δ^{18}O and δ^2H of water samples collected during August 2021.

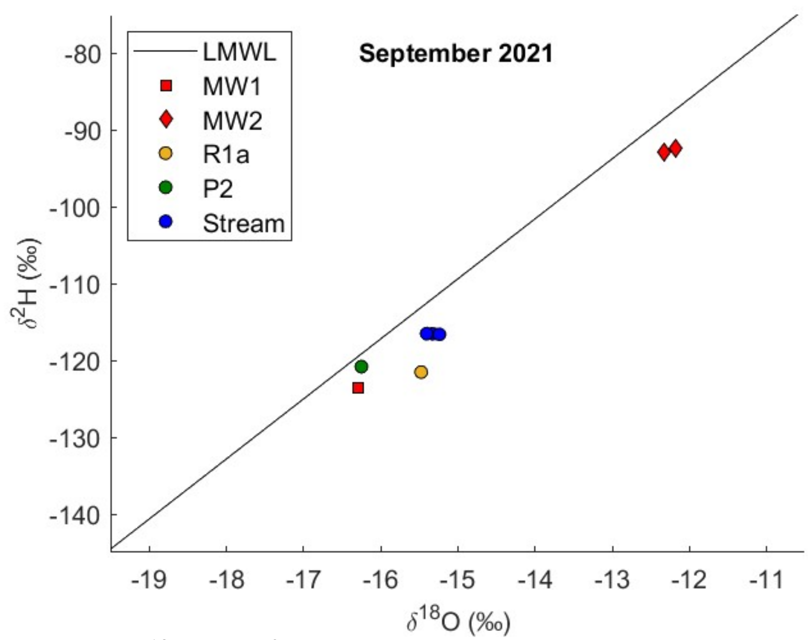

Figure A8: δ^{18}O and δ^2H of water samples collected during September 2021.

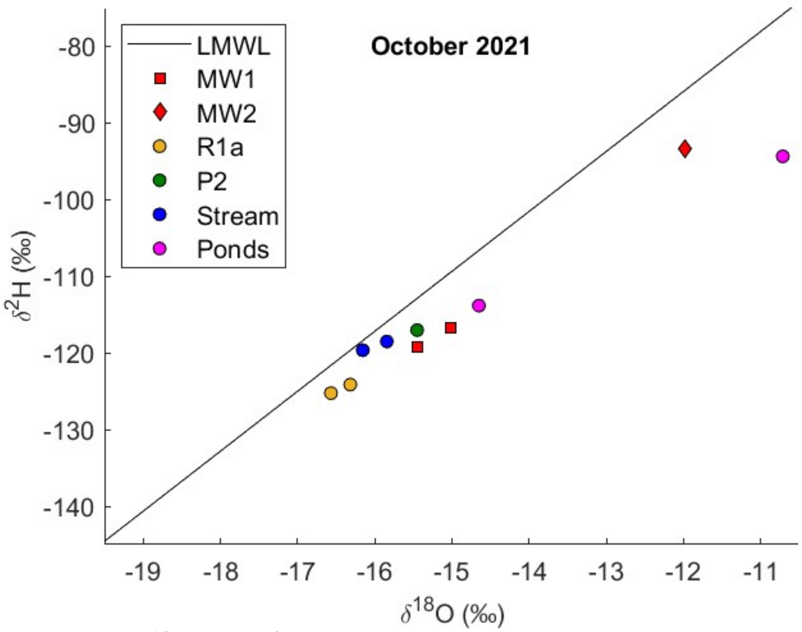

Figure A9: $\delta^{18}O$ and $\delta^{2}H$ of water samples collected during October 2021.

APPENDIX B

Table B1: Monthly average water level elevation (m amsl) in monitoring wells during May to October 2020. These values were used as targets for the transient model.

	May	June	July	August	September	October
R1a	2747.4	2747.5	2747.4	2747.4	2747.3	2747.3
R1b	2747.9	2748.0	2747.8	2747.6	2747.6	2747.5
MW1	2748.1	2748.2	2748.1	2747.8	2747.7	2747.6
R2a *	-	2743.9	2743.6	2743.5	2743.4	2743.3
R2b *	2743.6	2743.9	2743.6	2743.5	2743.4	2743.3
MW2	2743.0	2743.1	2743.1	2743.0	2742.9	2742.8

Notes:
*R2a and R2b levels are from 2021 due to a lack of data at these wells in 2020.